Ore Geology Reviews 91 (2017) 246–263

Contents lists available at ScienceDirect

Ore Geology Reviews

journal homepage: www.elsevier.com/locate/oregeorev

The unique Katugin rare-metal deposit (southern Siberia): Constraints on age and genesis

D.P. Gladkochub[a,*], T.V. Donskaya[a], E.V. Sklyarov[a,b], A.B. Kotov[c], N.V. Vladykin[d], S.A. Pisarevsky[e], A.M. Larin[c], E.B. Salnikova[c], V.B. Saveleva[a], V.V. Sharygin[f], A.E. Starikova[f], E.V. Tolmacheva[c], S.D. Velikoslavinsky[c], A.M. Mazukabzov[a], E.P. Bazarova[a], V.P. Kovach[c], N.Yu. Zagornaya[c], N.V. Alymova[d], E.A. Khromova[g]

[a] Institute of the Earth's Crust, Siberian Branch of the Russian Academy of Sciences, Irkutsk 664033, Russia
[b] Far East Federal University, Vladivostok 690091, Russia
[c] Institute of Precambrian Geology and Geochronology, Russian Academy of Sciences, St. Petersburg 199034, Russia
[d] A.P. Vinogradov Institute of Geochemistry, Siberian Branch of the Russian Academy of Sciences, Irkutsk 664033, Russia
[e] Earth Dynamics Research Group, ARC Centre of Excellence for Core to Crust Fluid Systems (CCFS) and The Institute for Geoscience Research (TIGeR), Department of Applied Geology, Curtin University, WA 6845, Australia
[f] V.S. Sobolev Institute of Geology and Mineralogy, Siberian Branch of the Russian Academy of Sciences, Novosibirsk 630090, Russia
[g] Geological Institute, Siberian Branch of the Russian Academy of Sciences, Ulan-Ude 670047, Russia

ARTICLE INFO

Keywords:
Katugin rare-metal ore deposit
Siberian Craton
Ta-Nb-Y-Zr (REE) mineralization
Geochemistry
Mineralogy

ABSTRACT

We report new geological, mineralogical, geochemical and geochronological data about the Katugin Ta-Nb-Y-Zr (REE) deposit, which is located in the Kalar Ridge of Eastern Siberia (the southern part of the Siberian Craton). All these data support a magmatic origin of the Katugin rare-metal deposit rather than the previously proposed metasomatic fault-related origin. Our research has proved the genetic relation between ores of the Katugin deposit and granites of the Katugin complex. We have studied granites of the eastern segment of the Eastern Katugin massif, including arfvedsonite, aegirine-arfvedsonite and aegirine granites. These granites belong to the peralkaline type. They are characterized by high alkali content (up to 11.8 wt% $Na_2O + K_2O$), extremely high iron content ($FeO^*/(FeO^* + MgO) = 0.96–1.00$), very high content of most incompatible elements – Rb, Y, Zr, Hf, Ta, Nb, Th, U, REEs (except for Eu) and F, and low concentrations of CaO, MgO, P_2O_5, Ba, and Sr. They demonstrate negative and CHUR-close $\varepsilon Nd(t)$ values of 0.0… − 1.9. We suggest that basaltic magmas of OIB type (possibly with some the crustal contamination) represent a dominant part of the granitic source. Moreover, the fluorine-enriched fluid phases could provide an additional source of the fluorine. We conclude that most of the mineralization of the Katugin ore deposit occurred during the magmatic stage of the alkaline granitic source melt. The results of detailed mineralogical studies suggest three major types of ores in the Katugin deposit: Zr mineralization, Ta-Nb-REE mineralization and aluminum fluoride mineralization. Most of the ore minerals crystallized from the silicate melt during the magmatic stage. The accessory cryolites in granites crystallized from the magmatic silicate melt enriched in fluorine. However, cryolites in large veins and lens-like bodies crystallized in the latest stage from the fluorine enriched melt. The zircons from the ores in the aegirine-arfvedsonite granite have been dated at 2055 ± 7 Ma. This age is close to the previously published 2066 ± 6 Ma zircon age of the aegirine-arfvedsonite granites, suggesting that the formation of the Katugin rare-metal deposit is genetically related to the formation of peralkaline granites. We conclude that Katugin rare-metal granites are anorogenic. They can be related to a Paleoproterozoic (~2.05 Ga) mantle plume. As there is no evidence of the 2.05 Ga mantle plume in other areas of southern Siberia, we suggest that the Katugin mineralization occurred on the distant allochtonous terrane, which has been accreted to Siberian Craton later.

1. Introduction

The Katugin Ta-Nb-Y-Zr (REE) deposit is located in the Kalar Ridge of Eastern Siberia, Russia (Fig. 1). This is one of the largest Precambrian Ta-Nb-Y deposits in the world and it belongs to the category of unique deposits containing industrial concentrations of ZrO_2 (1.51%), Nb_2O_5

* Corresponding author at: Institute of the Earth's Crust, Siberian Branch of the Russian Academy of Sciences, 128 Lermontov Str., Irkutsk 664033, Russia.
E-mail addresses: dima@crust.irk.ru, gladkochub@mail.ru (D.P. Gladkochub).

http://dx.doi.org/10.1016/j.oregeorev.2017.10.002
Received 23 September 2016; Received in revised form 4 October 2017; Accepted 6 October 2017
Available online 07 October 2017
0169-1368/

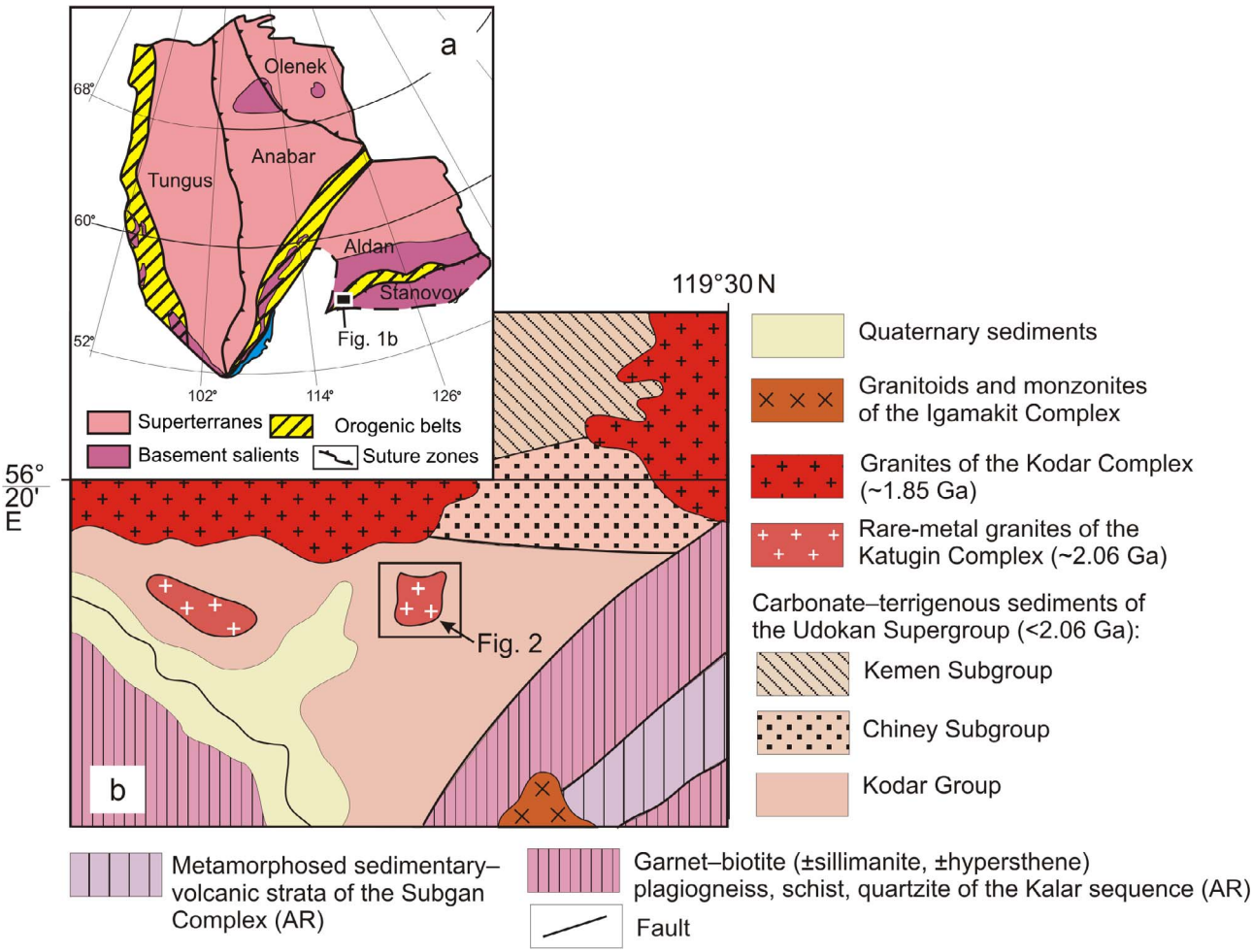

Fig. 1. The major tectonic elements of the Siberian craton, modified after Gladkochub et al. (2006) and Rosen (2003) (a); schematic geological map of the Udokan subzone of the Kodar–Udokan trough, modified after Podkovyrov et al., 2006 (b).

(0.30%), Ta_2O_5 (0.026%), Y_2O_3 (0.16%), U and REE (Arkhangel'skaya et al., 1998). One segment in the southern part of the deposit is extremely enriched in Ta_2O_5 (> 1.0% in average) (Pirajno and Santosh, 2014).

The Katugin deposit was discovered in the middle of the 20th century and has been explored over several decades. As most of the deposit is poorly exposed, tens of exploration holes have been drilled, two exploration tunnels and tens of trenches have been excavated. Prospecting and an economic appraisal of the Katugin deposit were completed in 1990s, with most of drill cores having been stored and used for new research. Any geological information about the Katugin deposit was hardly available to the international community until recently – most having been published in "grey" literature (e.g. internal reports). The only valuable exception was the paper of Arkhangel'skaya et al. (1993), but it was detailed enough for a comprehensive understanding of the genesis and specific aspects of the deposit. From the very beginning of its exploration the Katugin deposit was considered to belong to a metasomatic type controlled by faults (Prokhorov and Sobachenko, 1985; Arkhangel'skaya et al., 1993). Meanwhile Larin et al. (2002) identified the ore-bearing and ore-controlling rocks as the A-type alkaline granites and determined their Paleoproterozoic age. The characteristics of these granites and ores have been analysed and reported in a series of recent publications (Levashova et al., 2014; Kotov et al., 2015a,b; Larin et al., 2015; Sklyarov et al., 2016). These workers argue in favour of a genetic relation between Nb-Ta-Zr-Y (REE) ores of the Katugin deposit and alkaline granites of the Katugin complex, as a counter to a previously published hypothesis of their metasomatic fault-related genesis.

Here we systematize those arguments and present new data about types and age of mineralization, and propose our hypothesis of the genesis of the unique Katugin Ta-Nb-Y-Zr (REE) deposit.

2. Geological background

The Siberian craton is richly endowed with rare-metal mineral deposits (see overviews of Seltmann et al., 2010; Pirajno and Santosh, 2014). The most famous – Tomtor, Zaschikhinskoe and Beloziminskoe deposits are related to carbonatite. Whereas others, such as Vishniakovskoe and Goltsovoe are considered to be related to rare-metal granite and pegmatite. However, these issues for the Katugin deposit are still under discussion.

The Katugin deposit is located in the northern margin of the Stanovoy suture zone which separates the Aldan Shield (southern part of the Siberian craton) and adjacent terranes of the Central Asian Orogenic Belt (Fig. 1a). The mineralization is localized in two rather small (3 and 18 km^2) areas (Fig. 1b), which were previously considered either as fault-related metasomatic zones (Arkhangel'skaya et al., 1993, 2012; Bykov and Arkhangel'skaya, 1995; Prokhorov and Sobachenko, 1985; Ryabtsev et al., 2006), or as a massifs of Paleoproterozoic alkaline granites of the Katugin complex (Larin et al., 2002, 2015; Levashova et al., 2014).

The eastern part of the massif (hereafter Eastern Katugin massif) is better exposed than its western part. Moreover, hundreds of bore-holes were drilled here and two adits were mined. In this study we present new data from the Eastern Katugin massif only.

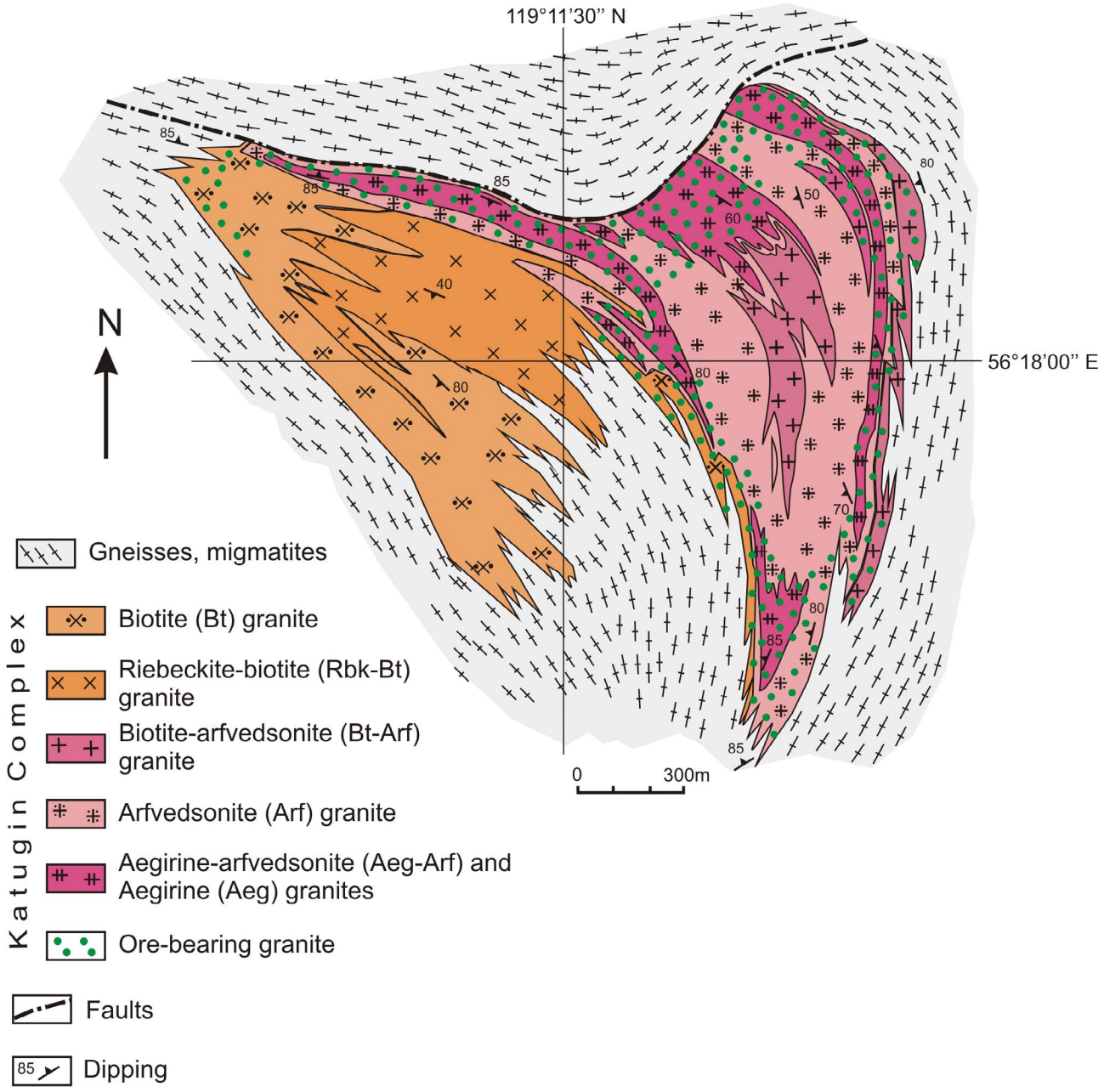

Fig. 2. Schematic geological map of the Eastern Katugin massif, modified after Prokhorov and Sobachenko (1985).

The Eastern Katugin massif has a curved heart-like shape and consists of two segments (Fig. 2). We have to note that the published maps (Arkhangel'skaya et al., 1993, 2012 etc), including the one used for our Fig. 2, are partly motivated by the metasomatic model of the massif's genesis and suffer from several contradictions. First, the metasomatite shape is overlain by granite and blastomylonite configurations without showing outlines of the bodies. Second, jagged contacts between different kinds of rocks hardly reflect the real situation, but mainly caused by difficulties in the correlation between boreholes and extensive complexity of the lithological varieties. Nonetheless, these maps are still useful for understanding the geometry and composition of the massif and related positions of ore bodies.

The eastern segment of the Eastern Katugin massif is composed by aegirine (Aeg), aegirine-arfvedsonite (Aeg-Arf), arfvedsonite (Arf) granites and to a less extent by biotite-arfvedsonite (Bt-Arf) granites. Biotite (Bt) and riebeckite-biotite (Rbk-Bt) granites compose the western segment, with biotite being dominant in the melanocratic rocks. Only the narrow contact zone in the northern part of this segment is composed by Arf and Aeg-Arf granites, and it is possible that this narrow strip is the continuation of the eastern segment.

Most of granites in the Eastern Katugin massif are medium- to fine-grained, but coarse-grained and even pegmatite-like varieties are also found in forms of cutting veins of irregular shapes with thicknesses of between 0.15 and 3 m. A foliation fabric of different extent is characteristic to all types of granites. Sometimes the foliation is visible only in a macroscopic scale (rocks look like normal massive granites under microscope), but more often the foliation is expressed in the microscopic level as well by lineation of biotite or arfvedsonite (aegirine) grains. Probably this widespread foliation was the reason for the initial hypothesis of the metasomatic genesis of the intrusive rocks. The occurrence of fragments of the host biotite gneisses within granites and their similar mineralogical composition probably also provoked a "metasomatic" hypothesis. A petrographic study of the foliated granites demonstrated that in most cases their foliation resulted during

emplacement, not during a metamorphic reworking. Dark minerals do not have any traces of re-crystallization and their composition is the same both in massive and in foliated rocks.

Fig. 2 clearly demonstrates that zonation from aegirine through amphibole to biotite rocks, suggested in earlier studies (Arkhangel'skaya et al., 1993, 2012), is only apparent. In fact the eastern segments of the intrusive massif, including the narrow northwestern strip, are mostly composed by Aeg, Aeg-Arf and Arf granites, whilst biotite and Rbk-Bt granites are dominant in the western segment. This could be explained by two pulses of granite emplacement.

3. Methods

> 120 samples of granites from the eastern segment of the Eastern Katugin massif have been collected to study their mineral and geochemical composition. Nine samples were taken to analyse the isotopic compositions of Nd, and to identify possible rock sources and to calculate their Nd-model age. We also made U-Pb zircon age determination of ore-segregations located among granites of the Eastern Katugin massif.

For the preliminary identification of minerals we analysed energy-dispersive spectra (EDS), back-scattered electron (BSE) images and elemental mapping (EDS system), using a TESCAN MIRA 3MLU scanning electron microscope equipped with a microprobe system INCA Energy 450 XMax-80 (Oxford Instruments Ltd) at the Institute of Geology and Mineralogy of the Siberian Branch of Russian Academy of Sciences (IGM SB RAS), Novosibirsk, Russia. Analytical parameters: high-vacuum mode, an accelerating voltage of 20 kV, a probe current of 1 nA, counting time of 20–60 s. Electron microprobe analyses (EMPA-WDS) of minerals have been carried out in IGM SB RAS, using a JEOL JXA-8100 electron microprobe. The operating conditions were as follows: beam diameter of 1–2 μm, accelerating voltage of 20 kV and a beam current of 10–15 nA, counting time of 10 s (for all elements). Precision for the major elements was better than 2%. For the data reduction we used the PAP routine (Pouchou and Pichoir, 1985).

We studied the content of Be, Li, B, Rb, Cs, Ba, Sr, Zr, Nb, Sn and H_2O in, amphibole, aegirine and astrophyllite of the Katugin deposit using the secondary-ion mass spectrometry (SIMS) on the Cameca IMS-4f ion probe in the Analytical Centre of the Yaroslavl Branch of the Institute of Physics and Technology (Yaroslavl, Russia). Only the previously analysed by EMPA > 20 μm grains have been used. Analysis of trace elements was carried out by the energy filter method; the operating conditions were as follows: primary O^{2-} beam – 20 μm, I = 2–4 nA, energy offset – 100 eV, and energy slit – 50 eV. Concentrations of elements were determined from the ratios of their isotopes to ^{30}Si, using calibration curves for standard samples (Jochum et al., 2000). The content of hydrogen has been determined from the ^{1}H mass together with trace elements. Low background content of H_2O (0.03 wt%) in the mass spectrometer was achieved by storing the samples for 24 h in high-vacuum. The NIST610 glass was used as an external standard.

Major elements and F in granites of the Eastern Katugin massif were determined by wet chemistry at the Centre for Geodynamics and Geochronology of the Institute of the Earth's Crust (Irkutsk). Al_2O_3 were analysed by atomic absorption spectroscopy (AAS) in samples of 14231, 14232, 14233, 14234, 14235, 14240, 14241, 14248, C-94-1, C-265-1, C-147-1, C-54-36 at the Vinogradov Institute of Geochemistry (Irkutsk). Trace elements and rare earths were determined by inductively coupled plasma mass spectrometry (ICP-MS) on an Agilent 7500ce (USA) at the Limnological Institute (Irkutsk). For ICP-MS the samples were fused with $LiBO_2$ following the procedure of Panteeva et al. (2003). Calibrations were with internal and international standards G-2, GSP-2, JG-2, and RGM-1. Analytical accuracy was 0.5–1.0% for major oxides and up to 5% for trace elements and REE.

Sm and Nd were extracted using the technique described by Kotov et al. (1995). Isotopic measurements were carried out at the IPGG RAS (St. Petersburg, Russia) using multicollector Triton T1 and Finnigan MAT 261 mass spectrometers. The measured $^{143}Nd/^{144}Nd$ values were normalized to $^{146}Nd/^{144}Nd = 0.7219$ and reduced to $^{146}Nd/^{144}Nd = 0.511860$ in the La Jolla Nd standard. The accuracy of the Sm and Nd measurements was 0.5%, and that of the $^{147}Sm/^{144}Nd$ and $^{143}Nd/^{144}Nd$ values was 0.005% (2σ). The average weighted $^{143}Nd/^{144}Nd$ value in the JNdi Nd standard derived from seven measurements is 0.512104 ± 8. The blank run was 0.03–0.2 and 0.1–0.5 ng for Sm and Nd, respectively. When calculating the values of the $\varepsilon_{Nd}(t)$ and model $t_{Nd}(DM)$ ages, we used the recent values accepted for the uniform chondrite reservoir CHUR (Jacobsen and Wasserburg, 1984) and depleted mantle DM (Goldstein and Jacobsen, 1988). For calculating two-stage model ages $t_{Nd}(DM\text{-}2st)$, the average crust value of $^{147}Sm/^{144}Nd = 0.12$ has been used.

Zircon separation was carried out following the standard procedures applying heavy liquids. Its morphological features were examined with the optic microscope (Leica DMPL) at 500–1000 times magnification ant with the ABT 55 and VEGA3 TES SCAN scanning electron microscopes employing secondary electron and cathodoluminescence detectors. The zircon crystals selected for U–Pb analysis were subjected to multistep removal of surficial contaminants using alcohol, acetone, and 1 M HNO_3. Between each step the zircons and their fragments were rinsed in ultrapure water. Chemical dissolution zircons and isolation of U and Pb were carried out following the modified method of Krogh (1973). In some cases in order to diminish the degree of discordance, an air-abrasive technique (Krogh, 1982) was applied. Isotope analyses have been performed using the multicollector Finnigan MAT 261 and Triton T1 mass spectrometers in both the static and the dynamic modes. The precision of determination of the concentrations of U and Pb as well as that of the Pb/U values was 0.5%. Blank contamination did not exceed 10 pg for Pb and 1 pg for U. The acquired raw data were processed with the PbDAT (Ludwig, 1991) and ISOPLOT software (Ludwig, 1999). For age calculation conventional U decay constants (Stacey and Kramers, 1975) were used. The correction for nonradiogenic lead was carried out in accordance with the model values (Steiger and Jager, 1976). All the errors presented are 2σ.

4. Petrography and mineralogy of the Katugin granites from the eastern segment of the Eastern Katugin massif

In the Katugin complex from the eastern segment of the Eastern Katugin massif the Bt-Arf, Arf, Aeg-Arf and Aeg granites are distinguished. The drill core study demonstrated that the Bt-Arf granites form isolated zones in the massif (see Fig. 2). The Aeg, Aeg-Arf and Arf granites interchange with each other, exhibiting gradual transition zones between purely aegirine and purely arfvedsonite granites, and the aegirine/arfvedsonite ratio sometimes changes significantly within short distances of 3–5 m. No Bt-Arf granites have been found in such zones. Despite the Bt-Arf granites being enriched in HFSE and REE, they cannot be considered as the ore-bearing rocks of the Katugin rare-metal deposit, so we do not discuss them any more in this study.

The studied Arf, Aeg-Arf and Aeg granites are mainly composed of quartz (20–35%), albite (20–30%) and K-feldspar (38–48%), in addition to mafic minerals (aegirine and arfvedsonite). All rock-forming, minor and accessory minerals of the Katugin granites are listed in Table 1. The Arf granites contain arfvedsonite (1–8%) as the only dark-colored mineral. Biotite is absent, rare small aegirite grains are found. The Aeg-Arf granites contain aegirine (1–8%) and arfvedsonite (1–8%) in various proportions – sometimes one of these minerals can be dominant, in other cases their content is equal. The content of aegirine in the purely Aeg granites is 3–8%. Some minor riebekite is found in the Aeg and Aeg-Arf granites, this mineral is clearly later than arfvedsonite and aegirine. Minor astrophyllite, bafertisite and polylithonite are locally recorded. Fe-chlorite is the major secondary mineral.

High concentrations of zircon and pyrochlore, as well as the presence of cryolite, are characteristic for the Aeg and Aeg-Arf granites.

Table 1
Minerals in Arf, Aeg-Arf and Aeg granites from the eastern segment of the Eastern Katugin massif, cryolitic rocks and as crystalline inclusions in zircons, modified after Sklyarov et al. (2016).

Mineral	Formula	Granites	Inclusions in Zrn	Cryolitic rocks
Quartz	SiO_2	+	+	+
K-feldspar	$KAlSi_3O_8$	+	+	+
Albite	$NaAlSi_3O_8$	+	+	+
Zircon	$ZrSiO_4$	+	−	+
Thorite	$ThSiO_4$	+	+	+
Polylithionite	$KLi_2AlSi_4O_{10}(F,OH)_2$	+	−	+
Hydrotetraferriannite	$(H_2O,K)Fe_3FeSi_3O_{10}(OH)_2$	+	−	−
Aegirine	$NaFeSi_2O_6$	+	+	+
Na-Fe-amphibole (group)	$(Na,K)Na_2Fe_4^{2+}Fe^{3+}Si_8O_{22}(F,OH)_2$	+	−	+
Astrophyllite	$(K,Na)_3(Fe,Mn,Zn)_7(Ti,Nb,Sn)_2Si_8O_{24}(O,OH)_7$	+	−	+
Bafertisite	$Ba_2(Ti,Sn)_2(Fe,Mn)_4(Si_2O_7)_2O_2(OH)_2(F,OH)_2$	+	−	+
Fe-chlorite	$(Fe^{2+},Fe^{3+})_5Al(Si_3Al)O_{10}(OH,O)_8$	+	+	−
Pyrochlore (group)	$(Ca,Na,REE,Y,Pb)_2Nb_2O_6(OH,F)$	+	+	+
Columbite-(Fe-Mn)	$(Fe,Mn)Nb_2O_6$	+	−	+
Fergusonite-(Y)	$YNbO_4$	+	+	−
Samarskite-(Y)	$(Y,Ce,U,Fe)_3(Nb,Ta,Ti)_5O_{16}$	+	+	−
Euxenite-(Y)	$(Y,Ca,Ce,U,Th)(Nb,Ta,Ti)_2O_6$	+	−	−
Ferberite	$(Fe,Mn)WO_4$	+	−	+
Pseudobrookite	Fe_2TiO_5	+	−	−
Pseudorutile	$Fe_2Ti_3O_9$	+	−	−
Ilmenite	$(Fe,Mn)TiO_3$	+	−	+
Magnetite	$FeFe_2O_4$	+	−	+
Rutile	TiO_2	+	−	+
Cassiterite	SnO_2	+	+	+
Cerianite-(Ce)	$(Ce,Th)O_2$	−	−	+
Goethite	$(Fe,Mn)O(OH)$	+	+	+
Siderite	$(Fe,Mn)CO_3$	+	+	+
Rhodochrosite	$(Mn,Fe)CO_3$	−	−	+
Calcite	$CaCO_3$	+	−	+
Bastnaesite-(Ce)	$(Ce,La,Nd)(CO_3)F$	+	+	+
Parisite-(Ce)	$Ca(Ce,La,Nd)_2(CO_3)_3F_2$	+	−	−
Synchysite-(Ce)	$Ca(Ce,La,Nd)(CO_3)_2F$	−	+	−
Fluorapatite	$Ca_5(PO_4)_3F$	+	−	−
Monazite-(Ce)	$(Ce,La,Nd)PO_4$	+	+	−
Xenotime-(Y)	YPO_4	+	+	−
Xenotime-(Yb)	$(Yb,Y)PO_4$	−	+	−
Cheralite-(Ce)	$(Ce,Th,Ca)(P,Si)O_4$	+	−	−
Barite	$(Ba,Sr)SO_4$	+	−	+
Galena	PbS	+	+	−
Sphalerite	ZnS	+	−	+
Molibdenite	MoS_2	+	−	−
Pyrrotite	$Fe_{1-x}S$	+	−	−
Pyrite	FeS_2	+	−	+
Chalcopyrite	$CuFeS_2$	+	−	+
Bornite	Cu_5FeS_4	+	−	−
Bithmutine	Bi_2S_3	+	+	−
Lead	Pb	+	−	−
Bismuth	Bi	+	+	−
Fluorite + Y-fluorite	$(Ca,Y)F_2$	+	+	+
Cryolite	Na_3AlF_6	+	+	+
Elpasolite	K_2NaAlF_6	−	−	+
Simmonsite	Na_2LiAlF_6	−	−	+
Tveitite-(Y)	$Ca_{1-x}Y_xF_{2+x}$, $x \approx 0.3$	+	+	+
«Ba-Sr-Tveitite-(Y)»	$(Ba,Sr,Ca)_{1-x}Y_xF_{2+x}$, $x \approx 0.3$	−	−	+
Gagarinite-(Y)	$NaCaYF_6$	+	+	+
Fluocherite-(Ce)	$(Ce,La,Nd)F_3$	+	+	+
Chiolite	$Na_5Al_3F_{14}$	−	+	+
Neighborite	$NaMgF_3$	−	−	+
Weberite	Na_2MgAlF_7	−	−	+
Usovite	$Ba_2CaMgAl_2F_{14}$	−	−	+
Ba- fluoraluminates	$BaAlF_4(OH)$, $BaCa_2AlF_9$, $BaCa_4AlF_{13}$	−	−	+
H_2O-OH-fluoraluminates	Prosopite, thomsenolite, pachnolite etc.	+	−	+

Note: +, mineral is present; −, mineral is absent.

Cryolite mostly occurs as streaks and disseminations, or as clusters in the Arf, Aeg-Arf and Aeg granites, but the large isolated cryolite lens-shaped 10 m thick body is found in the eastern segment of the Eastern Katugin massif. This body has been traced through 200 m along strike.

The dark-colored minerals have similar chemical composition in various types of the alkaline granites. The chemical compositions of minerals from the granites are given in the tables in Supplementary material. The arfvedsonite contains 0.7–1.1 wt% TiO_2, and the concentration of K_2O varies from 1.4 to 1.7 wt%. There are also significant amounts of ZnO (0.2–2.9 wt%), MnO (0.6–1.5 wt%), SnO_2 (0.1–0.7 wt %), Li_2O (0.5–0.9 wt%). We should also note a high content of F in amphiboles (up to F-arfvedsonite). Riebeckite is chemically different from arfvedsonite, mostly by significantly lower content of TiO_2 (< 0.3 wt%) and K_2O (< 0.2 wt%), and very low concentrations of

Table 2
Major- and trace-element compositions of granites from the eastern segment of the Eastern Katugin massif.

Sample	14216	14217	14220	14221	14226	14231	14232	14233	14234
Granite	Aeg	Arf	Aeg-Arf	Aeg-Arf	Arf	Aeg-Arf	Aeg-Arf	Aeg-Arf	Aeg-Arf
Location	Adit 1					Hole 107			
SiO_2, wt%	72.71	74.23	73.92	73.92	70.31	71.83	70.38	70.23	68.16
TiO_2	0.87	0.19	0.05	0.07	0.07	0.25	0.22	0.28	0.23
Al_2O_3	8.33	10.69	10.05	11.23	11.16	9.70*	10.40*	10.50*	11.20*
Fe_2O_3	3.30	2.04	2.06	2.17	2.27	2.35	2.69	2.11	2.35
FeO	1.14	2.06	2.06	2.31	3.29	2.15	2.37	2.91	2.12
MnO	0.06	0.04	0.04	0.03	0.06	0.04	0.04	0.07	0.04
MgO	< 0.02	< 0.02	< 0.02	< 0.02	< 0.02	0.05	0.10	0.09	0.07
CaO	< 0.02	< 0.02	< 0.02	< 0.02	< 0.02	< 0.02	< 0.02	< 0.02	< 0.02
Na_2O	3.43	4.01	5.41	4.53	5.56	5.89	6.20	5.38	6.22
K_2O	3.87	4.11	3.87	4.11	3.97	4.07	4.25	4.92	5.27
P_2O_5	< 0.03	< 0.03	< 0.03	< 0.03	< 0.03	< 0.03	< 0.03	< 0.03	< 0.03
H_2O^-	0.01	0.07	< 0.01	< 0.01	< 0.01	0.08	0.07	0.09	0.08
LOI	0.72	0.96	1.01	0.42	1.21	0.96	0.73	1.06	0.91
CO_2	< 0.06	< 0.06	< 0.06	< 0.06	< 0.06	< 0.06	0.06	< 0.06	< 0.06
F	0.70	0.78	1.73	0.34	1.40	2.50	2.48	1.87	1.60
-O	0.29	0.33	0.73	0.14	0.59				
Rb, ppm	1276.15	1090.87	810.86	793.73	628.54	1292.57	1178.00	1012.85	1154.41
Sr	24.12	39.84	9.12	1.72	20.25	14.40	13.46	12.72	6.96
Y	625.70	94.85	38.91	23.53	22.65	133.03	55.71	122.23	45.30
Zr	27845.97	6570.14	2389.40	2562.07	8184.85	3073.01	3042.39	4346.71	4996.24
Nb	4190.89	2942.99	1255.81	1260.84	2287.48	4471.05	3108.15	3068.32	3202.29
Ba	119.66	223.03	19.45	32.33	62.88	30.23	46.68	35.47	31.98
La	159.38	136.88	63.69	50.26	82.03	208.05	145.47	141.64	169.63
Ce	479.99	457.10	202.05	165.61	282.05	667.10	482.76	452.00	527.70
Pr	65.65	56.39	23.93	19.15	35.56	83.42	58.49	60.03	65.93
Nd	257.28	189.98	78.24	55.61	121.74	280.43	196.55	223.60	228.16
Sm	104.30	43.10	17.47	12.74	26.62	67.61	44.67	69.95	54.45
Eu	4.36	1.50	0.63	0.39	0.85	2.40	1.53	2.78	1.81
Gd	101.64	32.45	13.65	8.62	16.36	52.23	31.34	61.15	34.68
Tb	24.41	5.44	2.42	1.59	2.44	9.26	5.13	9.78	5.05
Dy	160.91	32.24	14.46	10.33	12.72	54.01	26.53	50.12	24.99
Ho	34.29	6.59	2.80	2.22	2.34	10.12	4.37	8.24	4.04
Er	87.97	18.50	7.33	6.78	6.84	25.01	9.62	14.72	9.26
Tm	12.14	3.03	1.23	1.26	1.23	3.70	1.45	1.74	1.48
Yb	78.64	21.80	9.75	10.68	9.49	23.96	12.25	10.78	12.53
Lu	13.34	3.74	2.03	2.04	1.68	4.20	2.60	2.06	2.81
Hf	1031.88	239.93	90.06	91.95	336.04	117.40	103.03	152.90	180.32
Ta	305.99	237.61	92.82	91.87	178.30	338.94	229.04	225.14	237.33
Th	277.11	63.24	21.58	31.96	40.76	82.36	43.40	36.34	43.88
U	121.94	108.66	42.17	39.38	100.02	156.70	103.99	109.21	110.75
A/NK	0.85	0.97	0.77	0.94	0.83	0.69	0.70	0.74	0.70
ASI	0.85	0.97	0.77	0.94	0.83	0.69	0.70	0.74	0.70
f	1.00	1.00	1.00	1.00	1.00	0.99	0.98	0.98	0.98
MALI	7.30	8.12	9.28	8.64	9.53	9.96	10.45	10.30	11.49
(La/Yb)n	1.31	4.06	4.23	3.04	5.59	5.62	7.68	8.50	8.76
Eu/Eu*	0.13	0.12	0.13	0.11	0.13	0.12	0.13	0.13	0.13
Ce/Ce*	1.05	1.16	1.15	1.19	1.16	1.13	1.17	1.09	1.11
(Gd/Yb)n	1.09	1.26	1.19	0.68	1.46	1.84	2.16	4.80	2.34
Sample	14235	K 52/14	C-107-17	14237	14238	14240	14241	C-84-13	C-84-12
Granite	Aeg	Aeg	Aeg-Arf	Aeg-Arf	Arf	Aeg	Aeg-Arf	Aeg-Arf	Arf
Location	Hole 107			Hole 84					
SiO_2,wt%	69.11	66.46	70.14	73.42	73.78	69.23	69.68	69.12	71.61
TiO_2	0.30	0.25	0.41	0.11	0.10	0.29	0.37	0.30	0.29
Al_2O_3	9.90*	10.70	9.52	10.90	11.53	8.80*	9.80*	10.41	10.63
Fe_2O_3	3.20	3.70	3.87	2.14	1.55	3.78	2.01	5.65	1.81
FeO	0.79	2.30	1.29	2.47	2.99	0.99	3.21	0.90	3.77
MnO	0.03	0.05	0.04	0.03	0.04	0.04	0.05	0.02	0.09
MgO	0.10	< 0.02	< 0.02	0.23	0.05	0.15	0.10	< 0.02	< 0.02
CaO	< 0.02	< 0.02	< 0.02	0.12	0.18	0.05	0.05	< 0.02	< 0.02
Na_2O	4.61	6.55	4.96	5.09	4.75	6.10	5.42	6.80	5.47
K_2O	4.77	3.63	3.56	4.30	4.47	3.60	4.28	3.58	3.63
P_2O_5	< 0.03	< 0.03	< 0.03	< 0.03	< 0.03	< 0.03	< 0.03	< 0.03	< 0.03
H_2O^-	0.12	0.15	< 0.01	0.08	0.06	0.10	0.07	0.07	0.12
LOI	0.57	0.93	0.21	0.28	0.16	0.85	0.87	1.13	1.13
CO_2	< 0.06	< 0.06	0.07	< 0.06	< 0.06	< 0.06	< 0.06	0.10	0.19
F	0.68	2.90	1.35	1.10	0.60	2.70	2.00	2.48	2.00
-O		1.22	0.57	0.46	0.25			1.04	0.84
Rb, ppm	2661.54	1345.96	1351.91	522.38	398.70	1225.04	1331.07	1571.06	655.93

(*continued on next page*)

Table 2 (*continued*)

Sample	14216	14217	14220	14221	14226	14231	14232	14233	14234
Granite	Aeg	Arf	Aeg-Arf	Aeg-Arf	Arf	Aeg-Arf	Aeg-Arf	Aeg-Arf	Aeg-Arf
Location	Adit 1					Hole 107			
Sr	13.69	15.69	2.11	30.72	14.42	7.73	12.43	27.88	35.60
Y	238.51	195.00	226.91	239.24	512.56	128.71	131.67	89.04	67.60
Zr	32431.20	22675.16	27901.51	302.15	1649.86	20610.03	12180.19	12506.29	10542.11
Nb	3878.81	3036.38	3447.60	232.14	297.61	2737.92	3973.07	2899.85	3765.21
Ba	27.83	8.46	21.77	53.29	55.49	30.60	36.34	40.40	57.23
La	141.71	184.51	187.98	240.18	237.60	120.20	186.71	127.57	210.65
Ce	456.80	447.36	597.94	522.41	514.24	387.90	584.73	432.86	683.28
Pr	61.33	55.75	69.38	59.45	61.42	50.69	76.78	48.48	73.43
Nd	224.69	204.68	252.37	222.47	227.83	179.24	281.41	167.49	241.89
Sm	70.37	49.25	79.76	56.46	61.00	49.56	79.87	43.69	55.94
Eu	2.54	2.27	3.55	2.21	2.42	1.74	2.92	1.78	1.97
Gd	54.21	46.63	80.03	54.19	64.07	34.18	57.40	33.45	37.58
Tb	11.67	10.11	15.80	8.04	11.40	6.23	10.17	5.58	5.37
Dy	76.89	71.10	96.25	47.57	73.77	42.28	54.91	36.07	32.16
Ho	17.02	14.35	18.71	9.63	16.83	9.61	9.71	7.13	5.72
Er	47.42	35.32	42.54	23.70	47.64	33.14	23.28	20.31	17.22
Tm	7.22	4.74	5.41	2.89	6.91	6.10	3.32	3.34	3.22
Yb	50.25	27.79	37.11	15.40	41.78	46.39	23.85	23.62	31.98
Lu	9.47	4.95	6.98	2.40	6.13	7.49	4.21	4.61	7.025
Hf	1359.89	705.69	951.19	11.89	64.46	794.62	463.27	393.65	320.66
Ta	342.10	293.14	248.20	18.13	21.73	239.42	332.58	228.56	280.36
Th	158.04	37.07	80.82	12.53	43.37	59.13	81.36	52.93	257.56
U	151.05	149.15	152.82	7.08	10.42	117.95	155.23	109.58	130.63
A/NK	0.78	0.73	0.79	0.84	0.91	0.63	0.72	0.69	0.82
ASI	0.78	0.73	0.79	0.82	0.89	0.63	0.72	0.69	0.82
f	0.97	1.00	1.00	0.95	0.99	0.97	0.98	1.00	1.00
MALI	9.38	10.18	8.52	9.28	9.04	9.65	9.65	10.38	9.10
(La/Yb)n	1.82	4.30	3.28	10.09	3.68	1.68	5.06	3.49	4.26
Eu/Eu*	0.13	0.15	0.14	0.12	0.12	0.13	0.13	0.14	0.13
Ce/Ce*	1.09	0.98	1.17	0.97	0.95	1.11	1.09	1.23	1.22
(Gd/Yb)n	0.91	1.42	1.82	2.98	1.30	0.62	2.04	1.20	0.99
Sample	14248	C-43-1	C-43-19	C-94-1	C-265-1	C-147-1	C-54-30	C-54-36	C-54-28
Granite	Aeg	Aeg-Arf	Aeg-Arf	Aeg-Arf	Aeg-Arf	Aeg-Arf	Arf	Arf	Arf
Location	Hole 43			Hole 94	Hole 265	Hole 147	Hole 54		
SiO_2,wt%	71.59	72.68	71.49	68.92	66.94	67.82	67.38	69.48	69.71
TiO_2	0.35	0.29	0.35	0.22	0.23	0.28	0.22	0.22	0.18
Al_2O_3	9.30*	10.90	8.98	11.90*	11.70*	11.20*	11.10	11.00*	10.67
Fe_2O_3	3.82	1.54	3.18	2.06	3.52	3.63	2.34	1.98	1.74
FeO	1.58	2.49	2.17	2.55	1.55	1.74	3.17	3.08	2.94
MnO	0.08	0.03	0.08	0.06	0.03	0.05	0.06	0.05	0.05
MgO	< 0.02	< 0.02	< 0.02	< 0.02	< 0.02	< 0.02	< 0.02	< 0.02	< 0.02
CaO	0.06	0.37	< 0.02	< 0.02	< 0.02	< 0.02	< 0.02	< 0.02	< 0.02
Na_2O	5.80	4.82	5.23	6.66	7.28	6.73	6.72	6.84	6.65
K_2O	4.06	4.27	3.71	4.53	4.52	4.50	4.26	3.75	4.11
P_2O_5	< 0.03	< 0.03	< 0.03	< 0.03	< 0.03	< 0.03	< 0.03	< 0.03	< 0.03
H_2O^-	0.04	< 0.01	1.85	0.07	0.05	0.07	0.16	0.04	0.23
LOI	0.98	0.05	0.67	0.96	0.92	1.00	1.57	1.33	1.61
CO_2	< 0.06	0.21	< 0.06	< 0.06	< 0.06	< 0.06	0.19	< 0.06	0.07
F	1.87	1.10	1.37	2.50	3.30	2.40	2.72	3.25	2.50
-O		0.46	0.58				1.15		1.05
Rb, ppm	1395.00	1608.70	1676.45	1157.19	1517.72	1783.84	819.48	706.76	801.33
Sr	14.58	8.19	8.32	24.50	43.47	37.24	16.00	23.44	13.35
Y	253.48	169.22	325.70	57.08	245.64	126.55	118.00	165.85	52.10
Zr	1597.18	13124.76	17105.76	488.05	4371.85	7304.63	3934.43	3090.62	2377.71
Nb	4454.89	3607.23	3760.97	3026.93	2681.75	2183.60	2459.10	2376.11	2203.17
Ba	35.72	35.57	21.59	23.42	114.09	14.67	17.38	21.44	22.01
La	171.89	197.00	137.35	142.98	134.27	98.04	196.32	178.61	128.02
Ce	539.42	643.21	498.88	503.21	457.87	339.46	616.88	571.10	423.00
Pr	72.17	72.18	58.74	58.84	56.02	42.23	69.51	65.32	47.87
Nd	266.20	253.13	219.13	211.50	202.94	155.79	238.07	235.53	156.86
Sm	85.78	70.23	69.22	48.15	56.21	45.05	52.72	54.24	35.58
Eu	3.29	2.85	2.96	1.60	2.05	1.57	1.88	2.06	1.11
Gd	68.32	59.63	68.00	35.12	43.27	33.53	40.84	43.45	24.92
Tb	14.76	11.45	13.80	4.99	9.17	6.43	6.78	7.42	4.11
Dy	93.72	72.86	94.85	27.91	61.56	44.34	41.13	45.71	24.60
Ho	18.49	12.46	18.83	4.27	13.46	9.68	7.86	9.05	4.20
Er	40.65	29.69	53.68	9.21	33.70	28.32	20.47	21.61	9.81
Tm	4.97	3.75	6.92	1.15	4.73	5.30	2.87	2.86	1.36
Yb	27.95	19.62	42.87	7.27	29.21	42.08	17.97	17.35	9.51
Lu	5.08	3.54	7.69	1.66	4.59	6.60	3.60	3.33	1.91

(*continued on next page*)

Table 2 (*continued*)

Sample	14216	14217	14220	14221	14226	14231	14232	14233	14234
Granite	Aeg	Arf	Aeg-Arf	Aeg-Arf	Arf	Aeg-Arf	Aeg-Arf	Aeg-Arf	Aeg-Arf
Location	Adit 1					Hole 107			
Hf	62.88	427.07	498.52	18.44	143.48	224.01	133.47	106.71	77.84
Ta	308.91	219.46	276.09	249.76	214.18	175.55	199.17	196.65	180.01
Th	255.27	131.47	215.34	43.87	83.02	64.38	50.90	34.97	24.18
U	145.84	127.08	119.83	110.21	99.89	83.87	114.69	95.52	80.62
A/NK	0.67	0.87	0.71	0.75	0.69	0.70	0.71	0.72	0.69
ASI	0.66	0.82	0.71	0.75	0.69	0.70	0.71	0.72	0.69
Fe index	1.00	1.00	1.00	1.00	1.00	1.00	1.00	1.00	1.00
MALI	9.80	8.72	8.94	11.19	11.80	11.23	10.98	10.58	10.76
$(La/Yb)_N$	3.98	6.50	2.07	12.73	2.97	1.51	7.07	6.66	8.71
Eu/Eu^*	0.13	0.14	0.13	0.12	0.13	0.12	0.12	0.13	0.11
Ce/Ce^*	1.08	1.20	1.24	1.22	1.18	1.18	1.18	1.18	1.20
$(Gd/Yb)_N$	2.07	2.57	1.34	4.09	1.25	0.67	1.92	2.12	2.22

Note: Aeg – aegirine granite; Aeg-Arf – aegirine-arfvedsonite granite; Arf – arfvedsonite granite.
A/NK = molar $Al_2O_3/(Na_2O + K_2O)$; ASI = molar $Al_2O_3/(CaO + Na_2O + K_2O)$; Fe index = $FeO^*/(FeO^* + MgO)$.
FeO^* = FeO + 0.8998 *x* Fe_2O_3; MALI = $Na_2O + K_2O$ – CaO; $Eu/Eu^* = Eu_N/\sqrt{(Sm_N\ x\ Gd_N)}$; $Ce/Ce^* = Ce_N/\sqrt{(La_N\ x\ Pr_N)}$; *N*, chondrite-normalized (Wakita et al., 1970). *, Al_2O_3 analysed by atomic absorption spectroscopy.

MnO and F.

Apart from an unusual emerald-green color, aegirine has a practically ideal composition – the content of Al_2O_3 does not exceed 1.3 wt%, and the content of CaO is less than 0.1 wt%. Only SnO_2 (up to 1.6 wt%) is present as a significant impurity.

Unlike the above mentioned minerals, astrophyllite may contain significant amounts of ore components, e.g. the content of ZrO_2 reaches 1.0 wt%, Nb_2O_5 is up to 5.0 wt%, Ta_2O_5 – up to 0.5 wt%. In addition, there are high concentrations of MnO (up to 2.7 wt%), Rb_2O (up to 2.0 wt%) and SnO_2 (up to 2.1 wt%).

5. Geochemistry of the Katugin granites from the eastern segment of the Eastern Katugin massif

The chemical composition of representative samples of Arf, Aeg-Arf and Aeg granites of the eastern segment of the Eastern Katugin massif are summarized in Table 2. All granites demonstrate elevated and high alkalinity ($Na_2O + K_2O$ = 7.3–11.8 wt%). The silica content in Arf, Aeg-Arf and Aeg granites varies from 66 to 74 wt%, which classifies these rocks in the TAS diagram (Sharpenok et al., 2013) as alkaline quartz syenites, alkaline granites and granites (Fig. 3a). The granites have A/NK [molar $Al_2O_3/(Na_2O + K_2O)$] = 0.63–0.97 and ASI [molar $Al_2O_3/(CaO + Na_2O + K_2O)$] = 0.63–0.97, which classifies them as peralkaline granites (Fig. 3b). According to Frost et al. (2001) all granites are ferroan (Fe index = 0.95–1.00), alkali and alkali-calcic (MALI [$Na_2O + K_2O$-CaO] = 7.3–11.8). Fig. 3a–d show the decreasing of the contents of $Na_2O + K_2O$ and of the MALI index, and some increase of the A/NK index with increasing of the SiO_2 content. The granites also have extremely low CaO contents (up to 0.37 ppm), MgO (up to 0.23 ppm), and P_2O_5 (< 0.03 ppm). On the other hand, the Arf, Aeg-Arf and Aeg granites are strongly enriched in F (0.34–3.30 wt%). Besides, there is a tendency for the Arf, Aeg-Arf and Aeg granites of the increasing of the Na_2O content with increased concentration of F, which is probably related to the amount of cryolite in the rock (Fig. 3e). There is also a positive correlation between Na_2O and Fe_2O_3tot, which is typical for the fractionated peralkaline silicic rocks (Scaillet and Macdonald, 2003; Costi et al., 2009) (Fig. 3f).

All granites have high concentrations of most incompatible elements (Rb, Y, Zr, Hf, Nb, Ta, Th, U, REEs), except for Eu. They are also characterized by low Sr and Ba concentrations. The spider diagram (Fig. 4a) shows the well-developed negative Ba, Sr, Eu, and Ti as well as positive Rb, Th, U, Nb, Ta, Zr, and Hf anomalies. Notably, the Arf, Aeg-Arf and Aeg granites have high but variable abundances of HFSE and REE, which is probably related to a random distribution of Zr-Hf, Nb-Ta and REE-bearing minerals in the granites. Extremely high contents of Zr (up to 32431 ppm), Hf (up to 1360 ppm), Nb (4471 ppm), Ta (339 ppm), total REE (up to 1584 ppm) occur in the Ae and Ae-Arf granites. The REE distribution in the granites is characterized by weakly and moderate enrichment in LREE ($[La/Yb]_N$ = 1.3–12.7) often with a slightly positive Ce anomaly (Ce/Ce^* = 0.95–1.24) and always with a negative Eu anomalies (Eu/Eu^* = 0.11–0.15) (Fig. 4b). The HREE segment demonstrate as positive as and negative slopes with $[Gd/Yb]_N$ = 0.62–4.80 (Fig. 4b).

The high concentrations of Rb with respect to those of Sr and Ba (Rb/Sr = 17–640; Rb/Ba = 5–159) are indicative the granite formation resulted from a deep differentiation of the parental melts. According to Frost and Frost (2008, 2011), Aeg, Aeg-Arf and Arf granites are peralkaline ferroan alkalic and alkali-calcic rocks, so they can be considered as differentiates of transitional in composition or alkali basaltic magma affected by some crustal contamination. Consequently a basaltic magma of transitional composition or OIB type can be considered as a source for Aeg, Aeg-Arf and Arf granites. Increasing of the A/NK index and decreasing of the MALI index with increased SiO_2, (Fig. 3c and d) – all these features suggest some contamination of the peralkaline differentiates by crustal melts during the formation of enriched SiO_2 granites. Overlapping of the compositions of Aeg, Aeg-Arf and Arf granites in all diagrams and similar trends are indicative for the same source for the granites.

Table 3 presents the results of Sm–Nd isotopic–geochemical investigations of the Arf, Aeg-Arf and Aeg granites as well as the ore segregations. They are characterized by negative and CHUR-close εNd (*t*) values of 0.0…−1.9 (Fig. 5) and usually by relatively high $^{147}Sm/^{144}Nd$ values. Therefore, the Nd model ages can be calculated only for two samples of granites ($T_{Nd}(DM)$ = 2.6–2.7 Ga). The two-stage Nd model age values ($T_{Nd}(DM\text{-}2st)$) of all samples are estimated between 2.5 and 2.7 Ga. The Aeg-Arf granite with SiO_2 = 74.2 wt% (maximum contents – see Table 3) has the lowest εNd(*t*) value of −1.9, which confirms our conclusion about the role of crustal contamination of the peralkaline differentiates during the formation of silica-enriched granites. Similar εNd(*t*) values and similar Nd model ages of the Arf, Aeg-Arf and Aeg granites and ore segregations suggest their common source.

6. The mineralization of the Katugin deposit

Most of the ore bodies located in the eastern segment of the Eastern Katugin intrusive massif. They are represented by the Arf, Aeg-Arf and Aeg granites, enriched in ore minerals, or by veins or lens-like bodies of the cryolite-rich rocks. The results of detailed mineralogical study suggest three major types of mineralization in the Katugin deposit. The

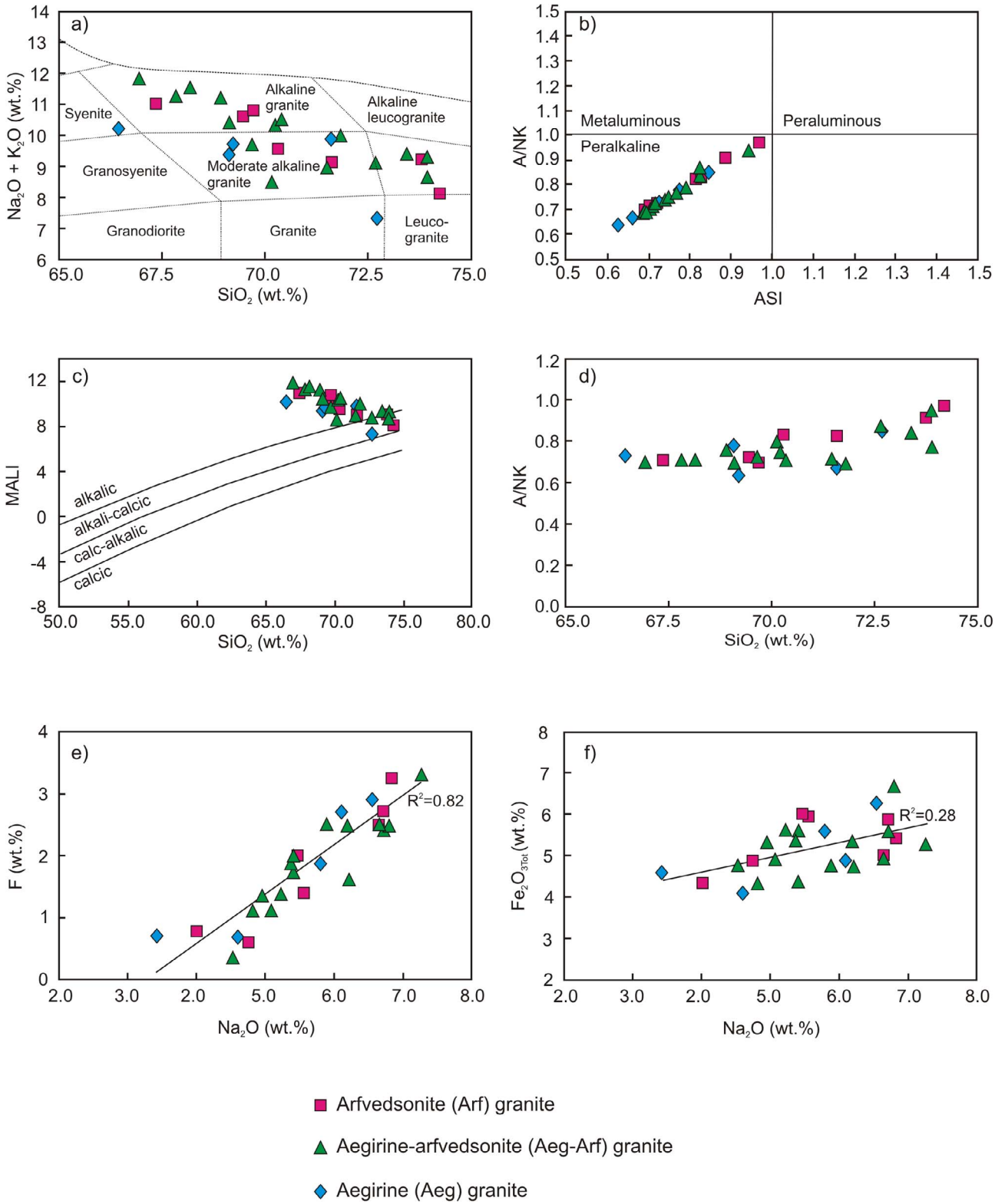

Fig. 3. ($Na_2O + K_2O$)–SiO_2 diagram of Sharpenok et al. (2013) (a), A/NK [molar $Al_2O_3/(Na_2O + K_2O)$] – ASI [molar $Al_2O_3/(CaO + Na_2O + K_2O)$] diagram (b), MALI [$Na_2O + K_2O$ – CaO] – SiO_2 diagram of Frost et al. (2001) (c), A/NK – SiO_2 diagram (d), F – Na_2O diagram (e), Fe_2O_3Tot – Na_2O diagram (f) for Arf, Aeg-Arf and Aeg granites of the eastern segment of the Eastern Katugin massif.

chemical compositions of ore minerals from the granites are provided in the Supplementary material.

6.1. Zr mineralization

Zircon is present in all rocks of the Eastern Katugin massif, but its amount varies from single crystals to the nest aggregates, containing up to 15–20% of the rock volume. Size of the crystals varies strongly from

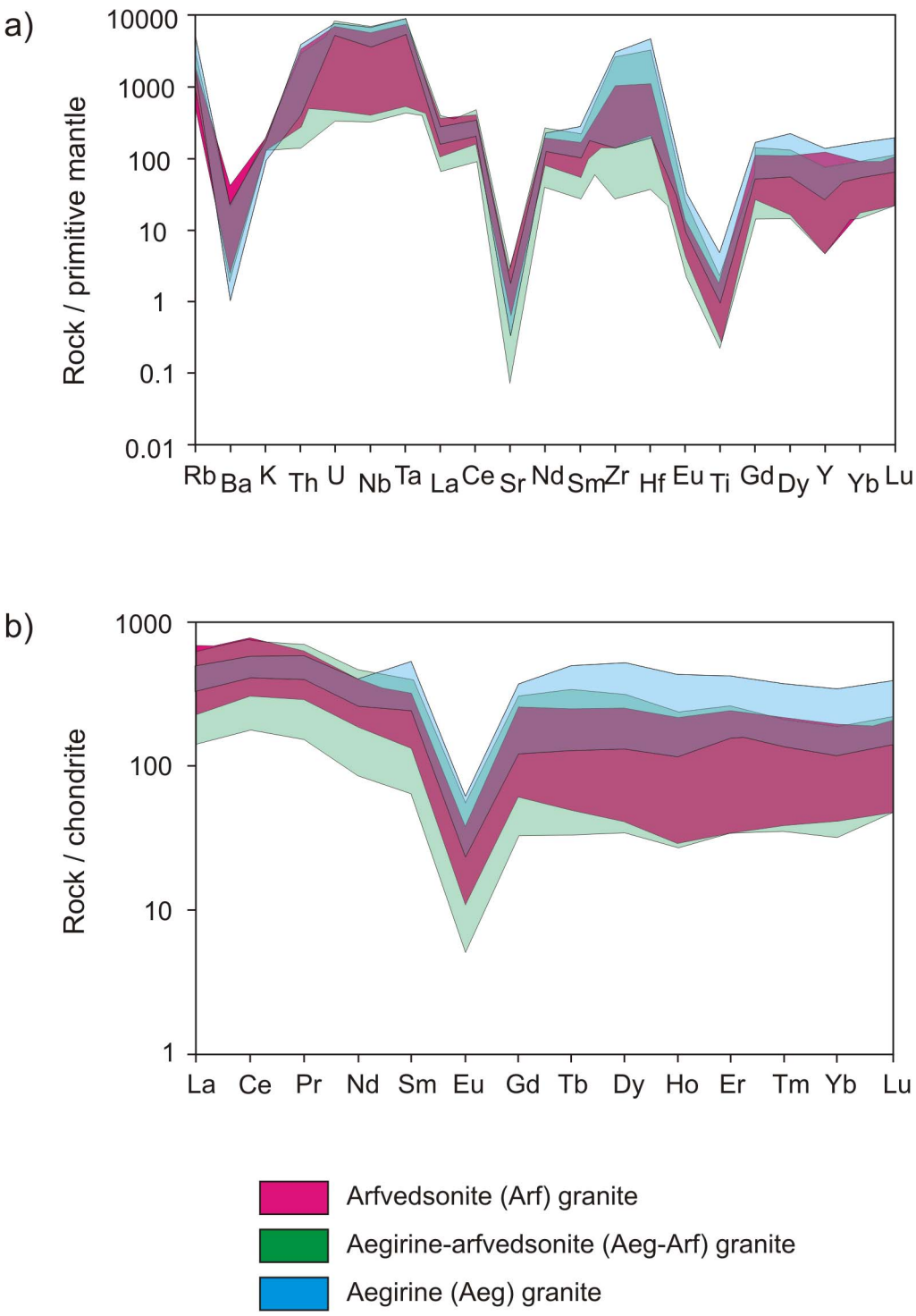

Fig. 4. Multi-element diagrams normalized to primitive mantle composition (Sun and McDonough, 1989) (a) and REE diagrams normalized to chondrite (Wakita et al., 1970) (b) for Arf, Aeg-Arf and Aeg granites of the eastern segment of the Eastern Katugin massif.

few micrometers to 1.5 cm (Arkhangel'skaya et al., 2012). Zircons in some cases are free of mineral inclusions, but in many cases contain tiny (2–15 μm) inclusions – predominantly quartz, bastnaesite, fluocerite, gagarinite, tveitite, ittrofluorite, thorite and cryolite (Fig. 6a and b). We suggest their syn-crystallization nature.

6.2. Ta-Nb-REE mineralization

Ta-Nb-REE minerals are present as: a) individual grains and aggregates in granites; b) inclusions in zircons (see above); c) interstitial aggregates among silicate minerals. Pyrochlore usually occurs as individual crystals or their aggregates and in most cases contains mineral inclusions and opaque rim (Fig. 6c). In most cases the crystals of pyrochlore have complex structure caused by variations in chemical composition or by inclusions of other minerals. Bastnaesite, columbite, fluocerite as well as hydrated pyrochlore are present in marginal parts of the crystals. Ore-mineral aggregates are usually composed of pyrochlore, columbite, fluocerite, ilmenite and sometimes sulphides (sphalerite, galena, pyrrotyte or pyrite) (Fig. 6d). Interstitial segregations consist of fluorides and fluocarbonates, sometimes with small amount of chlotite. Tveitite with numerous oriented inclusions of fluocerite or early bastnaesite, predominates (Fig. 6e and f). Late bastnaesite usually

Table 3
Sm–Nd isotopic data for granites and ore segregations the Eastern Katugin massif.

Sample	Rock type (SiO_2, wt%)	T, Ma	Sm (ppm)	Nd (ppm)	$^{147}Sm/^{144}Nd$	$^{143}Nd/^{144}Nd \pm 2\sigma$	$\varepsilon_{Nd}(T)$	$T_{Nd(DM)}$	$T_{Nd(DM\text{-}2st)}$
13023	Arf (72.9)	2066	30.1	143.9	0.1263	0.511656 ± 8	−0.5	2583	2548
14382	Aeg-Arf (67.6)	2066	63.1	234.0	0.1630	0.512156 ± 5	−0.4		2547
C-6-1	Arf (72.7)	2066	32.9	128.1	0.1551	0.512044 ± 2	−0.5		2554
C-15-1	Aeg-Arf (74.2)	2066	78.5	167.4	0.2837	0.513723 ± 2	−1.9		2667
C-38A-1	Aeg-Arf (72.7)	2066	73.2	195.4	0.2266	0.513014 ± 2	−0.6		2558
C-54-36	Arf (69.5)	2066	55.5	216.0	0.1557	0.511994 ± 2	−1.7		2648
C-94-1	Aeg (68.9)	2066	52.6	219.0	0.1452	0.511907 ± 2	−0.6		2559
C-54-27	Ore (64.6)	2066	153.7	671.0	0.1385	0.511780 ± 3	−1.3	2751	2616
C-121-1	Ore (64.7)	2066	184.9	642.0	0.1740	0.512331 ± 2	0.0		2507

Note: Rock types are Arf (arfvedsonite granite), Aeg-Arf (aegirine-arfvedsonite granite), Aeg (aegirine granite), Ore (ore segregation).

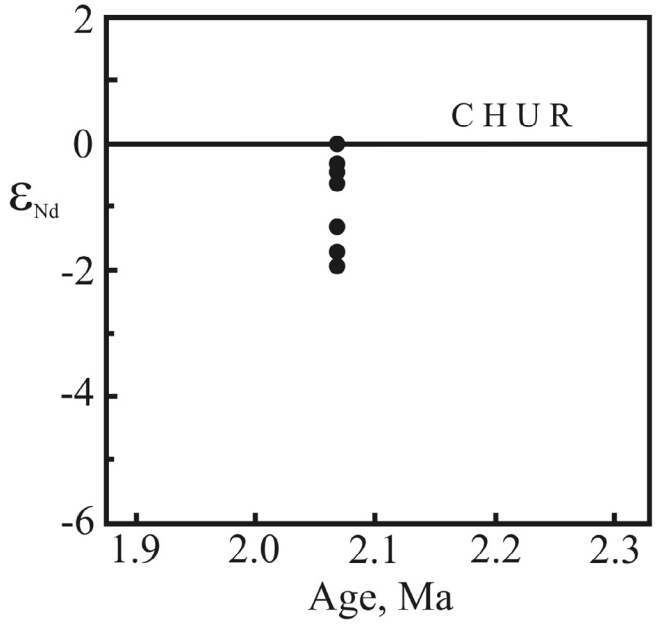

Fig. 5. The εNd(*t*) – age diagram for Arf, Aeg-Arf and Aeg granites and the ore segregations of the eastern segment of the Eastern Katugin massif.

develops after fluorides, composing small veins and individual aggregates, sometimes – symplectites with chlorite.

The composition of pyrochlores varies significantly even within a single grain in all rock types. The content of microlite (#Ta) in pyrochlores is relatively small – about 1–4%. Maximum variations are found for uranium (1–12 wt% UO_2) and lead (0–24 wt% PbO). Small amounts of Ta (0.5 wt% Ta_2O_5) are found in columbite. Only light REE are present in significant amounts in bastnaesites, but small amounts of thorium are also found (up to 3 wt% ThO_2).

Fluorides (fluocerite, tveitite, gagarinite, Y-fluorite) occur as clusters with or without cryolites in granites (see below), but sometimes as inclusions in zircons. Tveitite show largest variations in chemical composition. Apart from a normal tveitite some Ba-tveitite is also found. Significant variations of the light/heavy (+Y) REE ratio are observed in gagarinite. The sum of light REE in gagarinites varies from 0 to 20 wt%. Only light REE and Th in detectable amounts are found in fluocerite.

6.3. Aluminum fluoride mineralization

Cryolite is a dominating mineral among fluoroaluminates of the Katugin deposit. Cryolite commonly forms small isolations in granites and larger veins or lens-like bodies of cryolite-rich (> 30–50 vol%) rocks (Arkhangel'skaya et al., 1993, 2012). This mineral associates with other fluoroaluminates and fluorides (weberite Na_2MgAlF_7, chiolite $Na_5Al_3F_{14}$, neighborite $NaMgF_3$, fluorite, tveitite-(Y), fluocerite-(Ce), gagarinite-(Y), ittrofluorite, elpasolite K_2NaAlF_6, simmonsite Na_2LiAlF_6) and products of their alteration (gearksutite $CaAlF_4(OH)\cdot H_2O$, prosopite $CaAl_2(F,OH)_8$, thomsenolite $NaCaAlF_6\cdot H_2O$, pachnolite $NaCaAlF_6\cdot H_2O$, ralstonite $Na_xMg_xAl_{2-x}(F,OH)_6\cdot H_2O$) (Bykov and Arkhangel'skaya, 1995; Arkhangel'skaya et al., 2012; Sharygin and Vladykin, 2014).

7. The age of the Katugin deposit origin

Ages of the host rocks and of the mineralization are of a crucial importance for the modelling of any mineral deposit. The crystallization age of the Aeg-Arf granite (Eastern Katugin massif) has been reported at 2066 ± 6 Ma (U–Pb TIMS zircon dating; Larin et al., 2002). Our new U–Pb ages of zircons extracted from the ore segregation in the Aeg–Arf granite of this massif (sample KTG-241) provide the time of the ore formation. The ore segregations in the studied granites are composed mostly of zircon and pyrochlore (Arkhangel'skaya et al., 1993).

The zircon grains extracted from the sample are mainly transparent to semitransparent, euhedral, occasionally subhedral (Fig. 7I–IV), from cherry to dark cherry and light pink colored. Rare colorless euhedral bipyramidal crystals are also present. In the transmitted light and in the CL images, the zircons demonstrate zoned cores and homogeneous rims (Fig. 7V–X) with a high intensity of luminescence (Fig. 7V). The cores are enriched in mineral, primary melt, gaseous, and fluid inclusions, while the rims are devoid of melt inclusions (Fig. 7VI–VIII). Fluid and gaseous inclusions are located predominantly at the core–rim boundaries (Fig. 7IV–IX) as well as in fractures penetrating both cores and rims (Fig. 7X). The results of thermobarogeochemical studies demonstrate that the homogenization temperature of melt inclusions in zircon is 760–780 °C.

For geochronological study, the most transparent and homogeneous single zircon grains of cherry and dark cherry colors were selected from size fractions 100–150 and 200 μm (Nos. 1–4, Table 4), and one colorless grain from size fraction 200 μm (No. 4, Table 4). Two of these zircon grains were air-abraded (Nos. 2 and 4, Table 4) with up to 20% of the grain being removed. In the concordia plot (Fig. 8), the data points form a discordia line with the upper intercept age of 2055 ± 7 Ma and the lower one corresponding to 973 ± 110 Ma (MSWD = 1.3). The morphological features of the zircons from the ore segregation in the Aeg–Arf granite of the Eastern Katugin massif containing primary melt inclusions suggest their crystallization from a melt. In considering the good fit of the $^{207}Pb/^{206}Pb$ ages obtained from both air-abraded and non-treated zircons, it is possible to conclude that the growth of the rims in the studied zircons is not related to any overlapping process, and reflect the time of crystallization of the melt, parental to the ore segregations.

The obtained age of 2055 ± 7 Ma for the zircons from the ore segregation coincides within the error limits with the estimated age of the crystallization of the Katugin Aeg-Arf granites (2066 ± 6 Ma, U–Pb zircon age, Larin et al., 2002). Notably the accessory zircons from the granites contain numerous inclusions of minerals of rare and REE

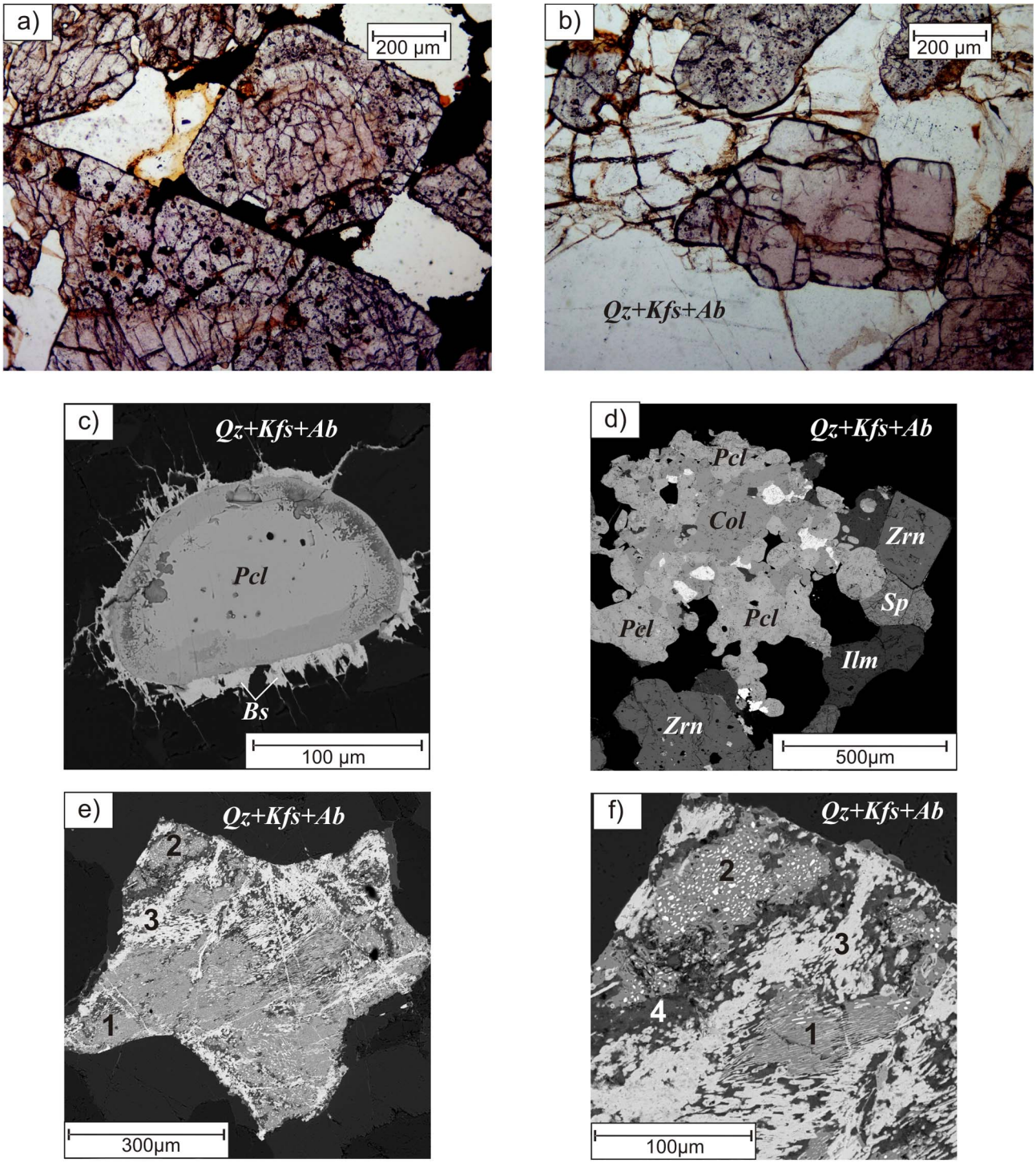

Fig. 6. Photomicrograph in plane polarized light (a and b) and backscattered electron images (c–f) of some ore minerals of the Katugin ore deposit. (a and b) – inclusion-rich and inclusion-free zircons in Aeg-Arf granite; (c) – pyrochlore grains rimmed by bastnaesite; (d) – ore-mineral aggregate, composed of pyrochlore, columbite, ilmenite and sphalerite; (e) – interstitial segregation, consisting of fluorides and fluocarbonates with small amount of chlorite; (f) – fragment of (e). Abbreviations: Bs – bastnaesite, Col – columbite, Ilm – ilmenite, Pcl – pyrochlore, Sp – sphalerite, Zrn – zircon, Qz – quartz, Kfs – K-feldspar, Ab – albite, 1 – tveitite with numerous fine oriented inclusions of early bastnaesite, 2 – tveitite with numerous fine oriented inclusions of fluocerite, 3 – late bastnaesite, 4 – chlorite with inclusions of late bastnaesite.

elements (bastnaesite, fluorite, Y–fluorite, fluocerite, monazite, thorite, synchisite, gagarinite, cryolite and others) (Levashova et al., 2014) and the same minerals often occur in ore segregations. We assume that formation of the Katugin deposit is genetically related to processes of formation of the Katugin alkaline granites.

8. Discussion

8.1. Magmatic nature of the mineralization of the Katugin deposit

Geological observations, geochemical characteristics of the granites and results of mineralogical, thermobarogeochemical and geochronological studies provide important evidence in favour of the magmatic models for the generation of rare-metal (and REE) enriched granite and,

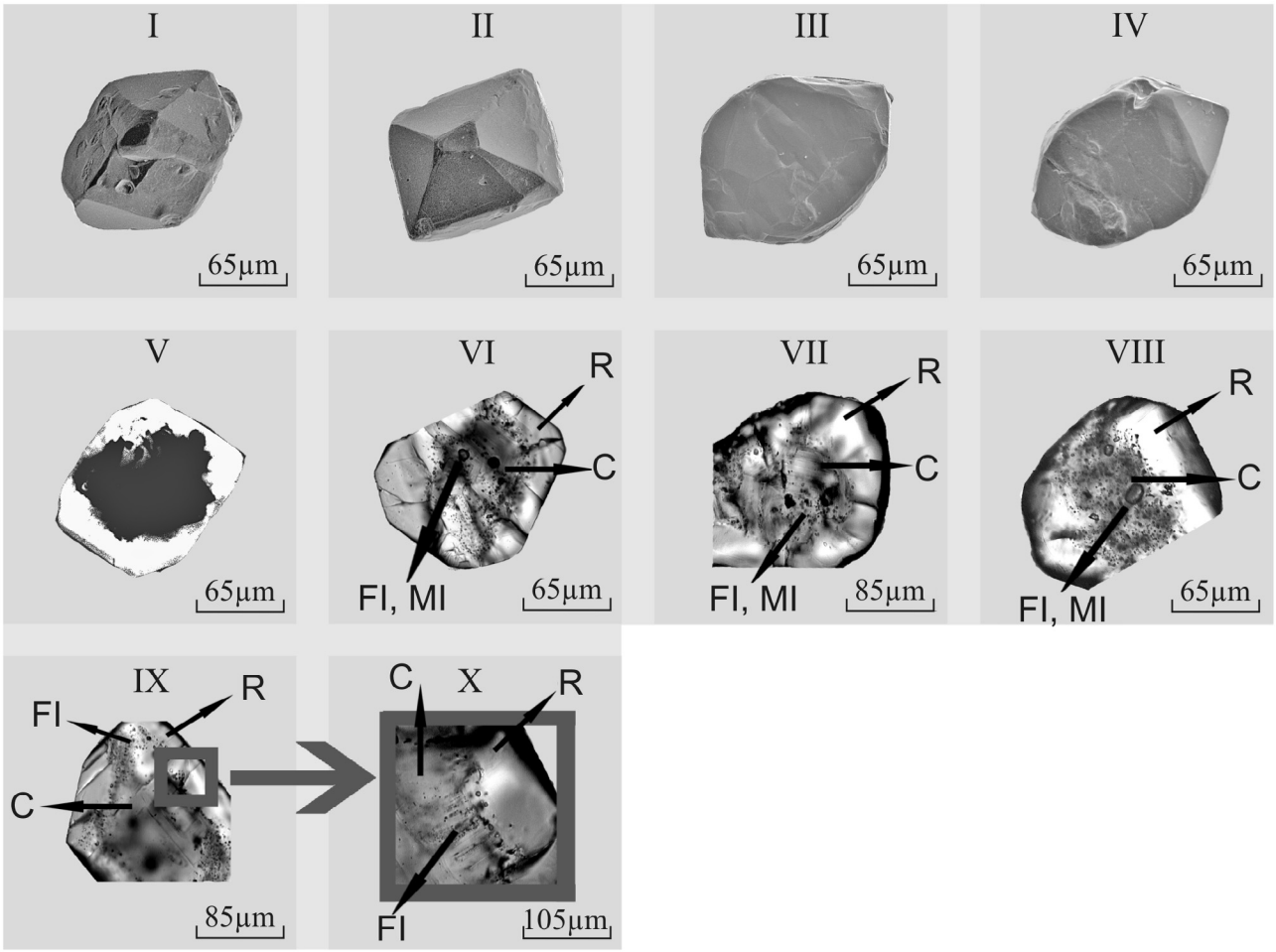

Fig. 7. Scanning electron microscope images of the zircon crystals from ore segregation (sample KTG-241) within Aeg-Arf granite: secondary electron – I–IV; cathodoluminescence – V; transmitted light optic microscope – VI–X. C – core; R – rim; FI – fluid inclusions; MI – melt inclusions.

consequently, for the genesis of the Katugin deposit, and allow to dismiss the hypothesis of the metasomatic origin of this deposit. We conclude that most of mineralization of the Katugin ore deposit occurred during the magmatic stage of evolution of the alkaline granitic melt, which had been a source for the Arf, Aeg-Arf and Aeg granites. The following lines of evidence support our conclusion.

1. Petrographic data clearly indicate that the ore minerals crystallized from the silicate melt during the magmatic stage. This is obvious for zircon, pyrochlore, gagarinite, ittrofluorite (both individual crystals and their monomineral aggregates), as well as for the polymineral aggregates of fergusonite, pyrochlore, fluocerite, ilmenite and sulphides. For example, zircons are found as inclusions in major minerals (e.g. albite, potassium feldspar and quartz) and pyrochlores sometimes occur as inclusions in albite. This is characteristic for the early magmatic stage of ore mineralization. Besides most of pyrochlore and bastnaesite crystals in granites contain high amount of F (3.32–5.50 and 8.13–8.64 wt%, correspondingly), which is also indicative for their crystallization in the magmatic stage (Yin et al., 2013; Huang et al., 2014).
2. Petrographic data show that the accessory cryolites in granites have been crystallized from the magmatic silicate melt enriched with fluorine. However, cryolites in larger veins and lens-like bodies have been crystallized at the latest stage from the fluorine salt melt (see below).
3. Thermobarogeochemical studies demonstrated that both rock-

Table 4
U-Pb isotopic data for zircons from the ore segregation in the Katugin aegirine–arfvedsonite granite (sample KTG–241).

No.	Grain size (μm) and their characteristics	U/Pb*	Isotopic ratios					*Rho*	Age, Ma		
			$^{206}Pb/^{204}Pb$	$^{207}Pb/^{206}Pb^{a}$	$^{208}Pb/^{206}Pb^{a}$	$^{207}Pb/^{235}U$	$^{206}Pb/^{238}U$		$^{207}Pb/^{235}U$	$^{206}Pb/^{238}U$	$^{207}Pb/^{206}Pb$
1	100–150, 1 grn, dark cherry-colored	1.84	257	0.1227 ± 3	0.5928 ± 1	5.7273 ± 211	0.3384 ± 7	0.84	1936 ± 7	1879 ± 6	1997 ± 4
2	> 200, *A* = 20%, 2 grn, cherry-colored	1.74	247	0.1254 ± 2	0.4684 ± 1	6.1623 ± 298	0.3565 ± 16	0.70	1999 ± 9	1965 ± 8	2034 ± 3
3	> 200, 1 grn, cherry-colored	1.96	301	0.1252 ± 4	0.3296 ± 1	6.2436 ± 250	0.3618 ± 7	0.51	2011 ± 8	1991 ± 4	2031 ± 6
4	> 200, *A* = 20%, 2 grn, cherry-colored	1.94	487	0.1257 ± 2	0.3764 ± 1	6.3099 ± 189	0.3640 ± 11	0.98	2020 ± 6	2001 ± 6	2039 ± 2
5	> 200, 1 grn, colorless	2.13	792	0.1256 ± 3	0.3553 ± 1	6.3254 ± 259	0.3654 ± 11	0.78	2022 ± 8	2008 ± 6	2037 ± 5

Note: [a], isotope ratios are corrected for blank and common lead; Rho, coefficient of correlation of $^{207}Pb/^{235}U$–$^{206}Pb/^{238}U$; *A*%, amount of matter removed by air-abrasion treatment; 2 grn, number of zircon grains used for U–Pb analysis; *, sample not weighed. Errors are 2-sigma and correspond to the last significant digits after the decimal point.

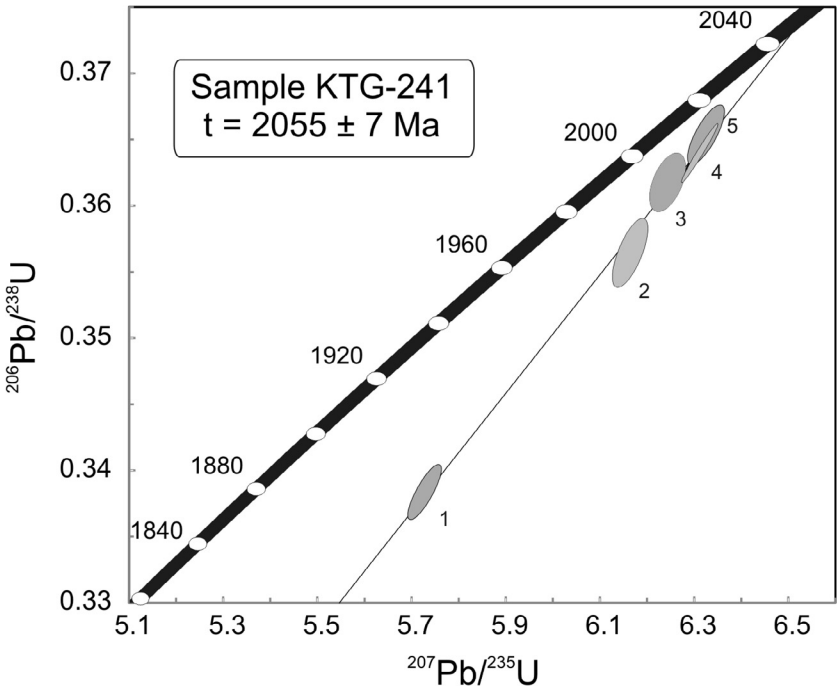

Fig. 8. Concordia diagram showing analyses of zircon from sample KTG-241. Spot numbers correspond to those in Table 4.

forming minerals of the granites (e.g. albite, quartz, and arfvedsonite) and accessory minerals (e.g. zircon and pyrochlore) contain syngenetic (primary) melt inclusions. These results demonstrate that the homogenization temperature of melt inclusions in zircon is 760–780 °C. Besides large salt-fluid inclusions (30–50 μm) are present in quartz (Kotov et al., 2015b).

4. Geochemical studies showed that the behaviour of such elements as Nb-Ta and Zr-Hf, which are parts of the ore minerals, mainly pyrochlore and zircon, has been controlled by magmatic processes. The well expressed linear positive Nb-Ta and Zr-Hf correlations are particularly indicative for that (Fig. 9a and b). Similar Nb/Ta = 10–16 and Zr/Hf = 24–34 ratios in the studied granites regardless of absolute concentrations of these elements are also in favour of the dominance of magmatic processes. In addition, the absence of correlation between SiO_2 and Nb, Zr, as well as between Na_2O and Nb, Zr (Fig. 9c–f), suggest very little influence of the post-magmatic (metasomatic) processes (e.g. greisenization, albitization) on the behaviour and distribution of these elements (Huang et al., 2014).
5. The 2066 ± 6 Ma U-Pb zircon age of the Aeg-Arf granites (Larin et al., 2002) is close to the 2055 ± 7 Ma zircon age of the ore segregation, suggesting that the formation of the Katugin rare-metal deposit is genetically related to the forming processes of the peralkaline granites.

8.2. A model proposed for the rare-metal Ta-Nb-Zr-REE mineralization of the Katugin deposit

Fluorine is the important factor (even a key factor) of the rare-metal (Ta-Nb-Zr-REE) enrichment of the acid melts, because the fluorine is a complexing agent for these elements, which is able to increase significantly their solubility (e.g., Manning, 1981; Charoy and Raimbault, 1994; Webster et al., 2004; Agangi et al., 2010; Moghazi et al., 2011). The Arf, Aeg-Arf and Aeg granites show high concentrations of F both in the rocks (up to 3.30 wt%) and in rock-forming and accessory minerals: arfvedsonite (up to 2.55 wt%), pyrochlore (up to 5.50 wt%) and bastnaesite (up to 8.61 wt%) This is likely related to dissolution of the fluorine in the magmatic melt at all stages of the magmatic evolution, including the late magmatic stage during the crystallization of the majority of ore mineral phases enriched by fluorine. Besides, some negative correlation between SiO_2 and F ($r = -0.72$) and consequently a small amount of fluorine in mostly felsic rocks indicates that the increasing of fluorine content in rocks is not related to post-magmatic hydrothermal processes. If the fluorine is added to a high temperature melt, it dissolves in it causing a decrease of the solidus temperature and changes in physical properties of acid magmas, in particular – a decrease of viscosity and an increase of diffusivity (Manning, 1981; Webster, 1990; Xiong et al., 1999; Scaillet and Macdonald, 2001; Lukkari and Holtz, 2007; Huang et al., 2014). Consequently a decrease of the solidus temperature causes a crystallization of major mineral phases at lower temperatures, which in turn makes Ta-Nb, Zr-Nb, REE incompatible to the melt and causes their assemblage to mineral complexes with the dissolved fluorine (Manning, 1981; Webster et al., 1989, 2004; Markl et al., 2001; Schönenberger et al., 2008; Agangi et al., 2010; Gramenitskiy et al., 2005; Shchekina et al., 2013; Dostal et al., 2014; Dostal and Shellnutt, 2016). At the early stages of magmatic crystallization these mineral complexes preserve their melt texture and are randomly distributed within magmatic system due to a low viscosity and high diffusivity of the F-rich granitic magma. Consequently they cannot crystallize at earliest stages, causing increase of the rare elements in the residual melt (Huang et al., 2014). Therefore, the majority of rare-metal accessory minerals crystallize mostly at the late magmatic stage.

8.3. A model for various types of cryolite segregation in the Eastern Katugin massif

The high content of cryolite is specific for the granites in the eastern segment of the Eastern Katugin Massif. This indicates high fluorine content in the source melts. As it was mentioned before, cryolite occurs in granites both as stringer disseminated pockets (accessory cryolie), and as larger veins or lens-like bodies of cryolite-rich rocks (latest magmatic cryolite). The accessory cryolite in granites occurs as inclusions in quartz, fills spaces between grains of leucocratic minerals, develops on the margins of feldspars and fills crevices in early magmatic albite and often in intergrowths with aegirine. Such petrographic data suggest a crystallization of the accessory cryolite from a granite melt enriched by fluorine, where cryolite is in equilibrium with main

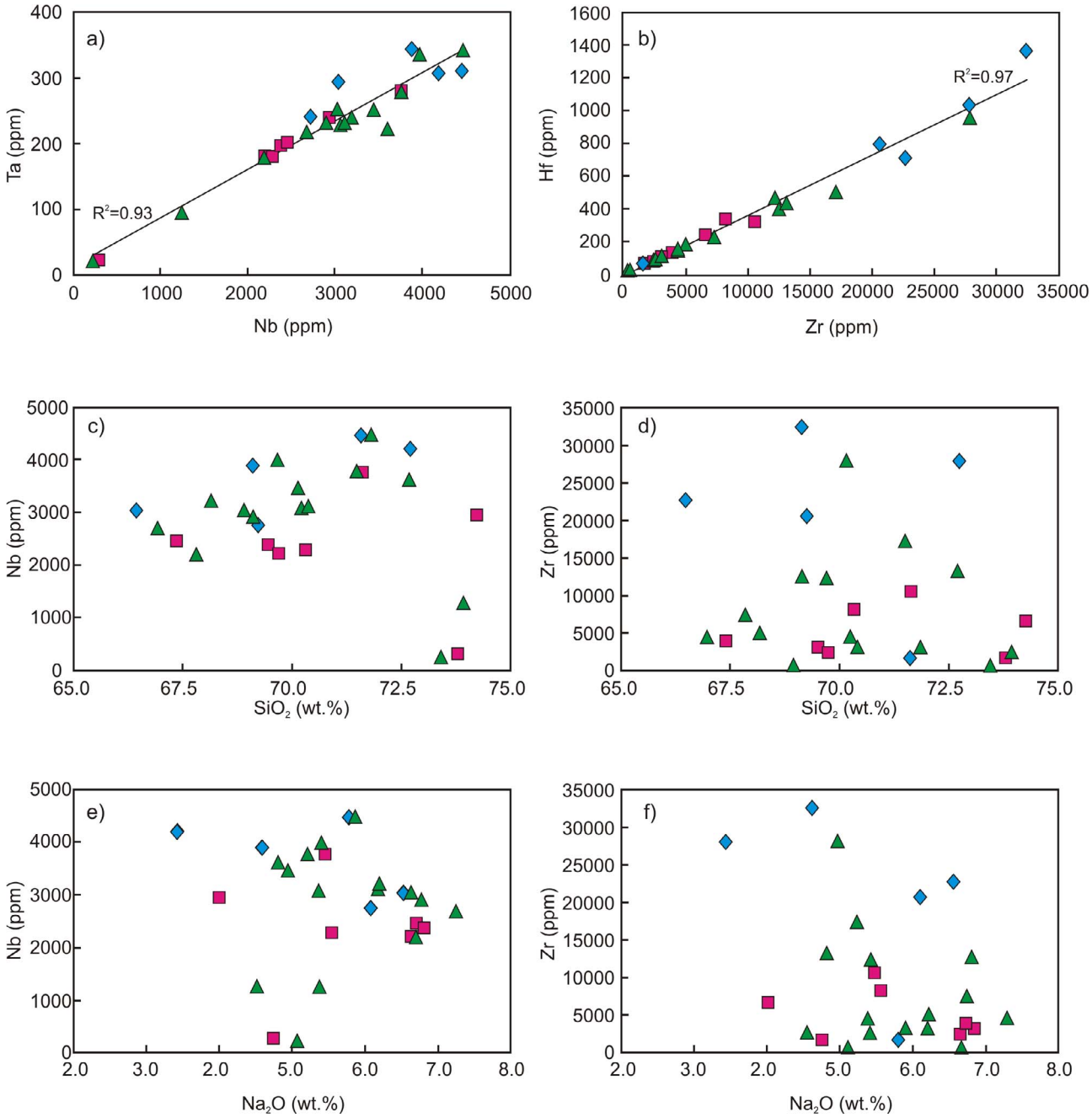

Fig. 9. Ta – Nb (a), Hf – Zr (b), Nb – SiO_2 (c), Zr – SiO_2 (d), Nb – Na_2O (e), Zr – Na_2O (d) for Arf, Aeg-Arf and Aeg granites of the eastern segment of the Eastern Katugin massif.

rock forming minerals (Shchekina et al., 2013). Good positive correlation between Na_2O and F in granites (Fig. 3e) suggests their coherent behaviour in the magmatic system. Apart from an accessory cryolite there are some larger veins or lens-like bodies of cryolite-rich rocks in the eastern segment of the eastern Katugin massif, which never extend outside of the massif. One of such bodies up to 10 m thick is reported from the southern part of the eastern segment. This body, apart from cryolite, contains crystals and intergrowths of arfvedsonite, annite, bafertisite, lepidolite, potassium feldspar, quartz, pyrochlore, gagarinite, tveitite, ilmenite, pyrite, sphalerite, magnetite and barite. Geological observations suggest that large cryolite bodies have been formed at the final stages of the formation of Katugin deposit, so we can consider them as largest magmatic bodies. Shchekina et al. (2013) demonstrated that such bodies could be formed during crystallization of cryolite from the fluorine salt melt separated from the aluminosilicate melt at the late stage of its differentiation. The residual melt crystallized later at lower temperatures than the silicate melt.

8.4. Source of the granites from the eastern segment of the Eastern Katugin massif

Peralkaline ferroan composition of the studied Afr, Aeg-Arf and Aeg granites, their isotopic ($\varepsilon Nd(t) = 0.0\ldots-1.9$) and geochemical (Y/Nb = 0.01–1.38, Rb/Nb = 0.17–2.25) characteristics suggest that basaltic magmas of OIB type (possibly with some influence of the crustal contamination) represent a dominant part of the granitic source. Enriched mantle source is supported by principal geochemical ratios, in particular by lower Th/Ta and Zr/Nb (0.1–2.0 and 0.4–8.4 correspondingly), indicating that this source was represented by the OIB-type mafic magmas (Larin et al., 2012). Strongly differentiated granite's compositions (Rb/Sr = 17–640, Rb/Ba = 5–159) indicate that the parent basaltic magmas should be produced at a high degree of the

fractional crystallization to achieve the stage of a granite melt. However the peralkaline silicic melt is not enough for the forming of rare-metal granitoids. The large amount of fluorine in the melt is also required. In spite of the increasing of the fluorine content during a progressive differentiation of the magmatic series of the felsic rocks, it is often not enough for the formation of large rare-metal deposits. We suggest that the fluorine-enriched magmatic fluid phases could provide an additional source of the fluorine. Dissolution of fluorine in the silicate melt has led to crystallization of rare metals and cryolites.

8.5. Tectonic setting of the Katugin rare-metal deposit

It is generally accepted that a great majority of large rare-metal deposits in the Earth are related to the alkaline rocks such as carbonatites, nepheline syenites and alkaline granites (see overview in Pirajno, 2009). According to modern ideas, either mantle plume, or sub-continental lithospheric mantle enriched in incompatible elements as the result of the plume-related activity, or of oceanic subduction, can be the sources for these rocks (Simonetti et al., 1998; Graham et al., 2004; Castor, 2008; Smith et al., 2016).

To decipher the geodynamic environments of the formation of the Katugin granites and of the Ta-Nb-Y-Zr (REE) deposit in particular, we have to consider the following: 1) analysis of the geological activity of the area in time of the granite emplacement, and 2) pertrological, geochemical and isotopic features of the granites.

The analysis of the evolution of superterranes in the southern Siberia and the distribution of major peaks in magmatic and tectonic activities in these superterranes (Gladkochub et al., 2009) demonstrate that the time around 2.06 Ga (the age of Katugin granites) belongs to the stagnant period of the anorogenic geodynamic environment. Apart from Katugin granites, the only magmatic rocks with ages between 2.20 and 2.06 Ga in the studied area are few picritic dykes (2204 ± 41 Ma, Sm-Nd mineral – whole rock, Puchtel and Zhuravlev, 1992) enriched in HFS elements. Such low magmatic activity on the wide areas of the southern part of the Siberian craton supports the hypothesis about the domination of anorogenic environments there with just minor extensional events (Larin et al., 2002; Kotov, 2003). Importantly the mentioned 2.20–2.06 Ga magmatic events expressed by picrite dykes and Katugin granites were not directly related to the formation of Siberian craton, but resulted from just local internal processes within terranes, which assembled after 1.88–1.85 Ga accretionary and collisional events.

The conclusion about the anorogenic nature of the studied rare-metal granites, which is based on geological data and on the likely scenario of the Siberian Craton's formation, is supported by geochemical data. Notably it is possible, that the anorogenic magmatism is often related to mantle plumes (Pirajno, 2015). Our geochemical and isotopic data support plume-related nature of the Katugin Massif. Interestingly there is no evidence for a coeval magmatic activity in other areas of anywhere in the Siberian craton (Gladkochub et al., 2009, 2010). This suggests that the mantle plume was most likely localized beneath the allochthonous terrane which hosts the Katugin deposit and that this terrane at ~2.05 Ga has not been connected to the southern part of the Siberian Craton, but developed and moved separately at some distance.

Felsic and alkaline magmatism was not wide spread at ~2.05Ga, but several large rare-metal deposits are associated with these types of magmatism. Apart from the Katugin deposit there are at least four other nearly coeval deposits. The closest analogue is the Canadian Thor Lake group of deposits. They are located in the southern part of the Archean Slave Craton near its margin within the ~2.0–1.8 Ga Thelon orogenic belt (e.g. Whitmeyer and Karlstrom, 2007; Buchan et al., 2010). Five deposits of this group with complex Zr, Nb, Ta, REE, Be and Ga mineralization, which belong to the unique category (Osokin et al., 2000), are associated with the alkaline to peralkaline Blachford Complex, related to a development of the Athapuscow aulacogen (Trueman and Pedersen, 1988). The age of the older part of this complex is 2175 ± 7 Ma, the age of the younger part – 2094 ± 10 Ma (Bowring et al., 1984). The rare-metal ores, which are associated with alkaline and nepheline syenites, have the similar age (Sheard et al., 2012). The alkaline rocks of the Blachford Complex have been formed in the extensional environments, which are indicated by the 2.03–2.02 Ma mafic dyke swarms (Buchan et al., 2009).

Mount Weld in Western Australia is another giant rare-metal (REE, Nb, Ta, Zr) deposit of similar age. The ore zone is a laterite developed after carbonatite in Quaternary time. The carbonatite intrusion cuts across the Archean volcano-sedimentary rocks of the Laverton tectonic zone and belongs to the Paleoproterozoic magmatic province, which includes alkaline intrusions of carbonatites and kimberlites (Duncan and Willett, 1990). The Re-Os age of the Mount Weld carbonatites is 2025 ± 10 Ma (Graham et al., 2004), and the Rb-Sr age is 2021 ± 10 Ma (Collerson, 1982).

The rare-metal deposits are also associated with the ~2060 Ma giant bimodal Bushveld Complex in South Africa (Kaapvaal Craton). The Lebowa Granite Suite, which is co-genetic with the mafic to ultramafic layered Rustenburg Series, forms a 2–3 km thick plate-like body in the central part of the complex. These alkaline granites are enriched in incompatible elements and belong to the intraplate A-type granites. The commercially exploitable Sn-fluorite, Sn-polymetallic, Mo-fluorite and uranium deposits are associated with these granites, while the layered series of the Bushveld Complex contains the world largest chromium, vanadium and PGE deposits. It is also possible to associate the alkaline-ultramafic intrusions and carbonatites of the Phalaborwa Complex with the Bushveld Complex – they are spatially close and have a similar age of 2047 ± 8 Ma (Eriksson, 1984). The Phalaborwa carbonatites are associated with commercially exploitable Cu, REE, U, Zr, Au and apatite mineralization (Harmer, 2000).

Interestingly the cratons on which the abovementioned ~2.05 Ga giant rare-metal deposits are found (i.e. Slave, Yilgarn and Kaapvaal) have been assigned by Bleeker (2003) to three different craton "clans" with little, if any similarities between them. Hence any paleogeographic affinity between these deposits is not very likely. However, the present state of the knowledge about the ~2.05 Ga global paleogeography is quite low, so any speculations on this matter are probably premature.

9. Conclusions

1. The geological, mineralogical, geochemical and geochronological data are indicative of the magmatic genesis of the giant Katugin rare-metal deposit rather than of previously suggested (Prokhorov and Sobachenko, 1985; Arkhangel'skaya et al., 1993, 1998) unique metasomatic fault-related origin.
2. The Ta-Nb-Y-Zr (REE) ores of the Katugin deposit are genetically related with the granites of the Katugin complex, mainly with arfvedsonite, aegirine-arfvedsonite and aegirine granites.
3. The studied Arf, Aeg-Arf and Aeg granites of the eastern segment of the Eastern Katugin massif correspond to peralkaline granite. They are characterized by high alkalinity, high iron content ($FeO^*/(FeO^* + MgO) = 0.96–1.00$), very high content of most incompatible elements – Rb, Y, Zr, Hf, Ta, Nb, Th, U, REEs (except for Eu) and F, and low concentrations of CaO, MgO, P_2O_5, Ba, and Sr. They demonstrate negative and CHUR-close $\varepsilon Nd(t)$ values of 0.0…−1.9. Some aegirine and aegirine-arfvedsonite granites have extremely high contents of Zr, Hf, Nb, Ta and total REE.
4. Basaltic magmas of OIB type (possibly with some influence of the crustal contamination) could be a dominant part of a source for Aeg, Aeg-Arf and Arf granites. Moreover, the fluorine-enriched fluid phases could provide an additional source of the fluorine. Strongly differentiated granite's compositions indicate that the parent basaltic magmas should be produced at a high degree of the fractional crystallyzation.
5. The results of detailed mineralogical study suggest three major types of ore-mineralization in the Katugin deposit: Zr mineralization

(zircon), Ta-Nb-REE mineralization (pyrochlore, bastnaesite, columbite, fluocerite, tveitite, gagarinite etc.) and aluminum fluoride mineralization (cryolite etc.).

6. Most of ore minerals crystallized from the silicate melt during the magmatic stage. The accessory cryolites in granites have been crystallized from the magmatic silicate melt enriched with fluorine. However, cryolites in large veins and lens-like bodies have been crystallized at the latest stage from the fluorine salt melt.
7. The zircons from ore segregation in the Aeg-Arf granite have been dated at 2055 ± 7 Ma. This age is close to the 2066 ± 6 Ma zircon age of the granites themselves (Larin et al., 2002), suggesting that the formation of the Katugin rare-metal deposit is genetically related to the forming processes of the peralkaline granites.
8. The geological and geochemical data prove an anorogenic nature of the Katugin rare-metal granites related to a Paleoproterozoic (~2.05 Ga) mantle plume occurred in the studied area.

Acknowledgments

The research was mainly supported by grant 14-17-00325 from the Russian Science Foundation. Mineralogical investigations were partly performed under support of grant No. 16-35-60054-mol-a-dk from the Russian Foundation for Basic Research (A.E.S.). This is contribution 1020 from the ARC Centre of Excellence for CORE to Crust Fluid Systems (http://www.ccfs.mq.edu.au) and contribution to IGCP 648.

Appendix A. Supplementary data

Supplementary data associated with this article can be found, in the online version, at http://dx.doi.org/10.1016/j.oregeorev.2017.10.002.

References

Agangi, A., Kamenetsky, V.S., McPhie, J., 2010. The role of fluorine in the concentration and transport of lithophile trace elements in felsic magmas: insights from the Gawler Range Volcanics, South Australia. Chem. Geol. 273, 314–325.
Arkhangel'skaya, V.V., Bikhovsky, L.Z., Peziruk, L.K., 1998. The Katugin Ta-Nb-Zr-Y-Tr mineral deposit – the object for possible investments. In: Laverov, N.P. (Ed.), Large and Unique Deposits of Rare Metals. SPBGGI, St. Petersburg, pp. 94–100 (in Russian).
Arkhangel'skaya, V.V., Kazanskii, V.I., Prokhorov, K.V., Sobachenko, V.N., 1993. Geological structure, zoning, and conditions of formation of the Katuginskoe Ta–Nb–Zr deposit (Chara–Udokam district, East Siberia). Geol. Ore Deposits 35, 115–131.
Arkhangel'skaya, V.V., Ryabtsev, V.V., Shuriga, T.N., 2012. Geological Structure and Mineralogy of the Tantalum Deposits of Russia. VIMS, Moscow (in Russian).
Bleeker, W., 2003. The late Archean record: a puzzle in ca. 35 pieces. Lithos 71, 99–134.
Bowring, S.A., Van Schmus, W.R., Hoffman, P.F., 1984. U-Pb zircon ages from Athapuscow aulacogen, East Arm of Great Slave Lake, N.W.T, Canada. Can. J. Earth Sci. 21, 1315–1324.
Buchan, K.L., Ernst, R.E., Bleeker, W., Davis, W.J., Villeneuve, M., van Breemen, O., Hamilton, M., Söderlund, U., 2010. Proterozoic Magmatic Events of the Slave Craton. Wopmay Orogen and Environs, Geological Survey of Canada, Open File, pp. 5985.
Buchan, K.L., van LeCheminant, A.N., Breemen, O., 2009. Paleomagnetism and U-Pb geochronology of the Lac de Gras diabase dyke swarm, Slave Province, Canada: implications for relative drift of Slave and Superior provinces in the Paleoproterozoic. Can. J. Earth Sci. 46, 361–379.
Bykov, Yu.V., Arkhangel'skaya, V.V., 1995. Katugin rare-metal deposit. In: In: Laverov, N.P. (Ed.), Transbaikalian Deposits, vol. 1 (2). Geoinformmark, Chita-Moscow, pp. 76–85 (in Russian).
Castor, S.B., 2008. The mountain pass rare-earth carbonatite and associated ultrapotassic rocks, California. Can. Mineral. 46, 779–806.
Charoy, B., Raimbault, L., 1994. Zr-, Th-, and REE-rich biotite differentiates in the A-type granite pluton of Suzhou (Eastern China): the key role of fluorine. J. Petrol. 35, 919–962.
Collerson, K.D., 1982. Age and Strontium Isotope Systematics of the Mt. Weld Carbonatite. Report to Union Oil Development Corporation, Western Australia unpublished.
Costi, H.T., Dall'Agnol, R., Pichavant, M., Rämö, O.T., 2009. The peralkaline tin-mineralized Madeira cryolite albite-rich granite of Pitinga, Amazonian craton, Brazil: petrography, mineralogy and crystallization processes. Can. Mineral. 47, 1301–1327.
Dostal, J., Kontak, D.J., Karl, S.M., 2014. The Early Jurassic Bokan Mountain peralkaline granitic complex (southeastern Alaska): geochemistry, petrogenesis and rare-metal mineralization. Lithos 202–203, 395–412.
Dostal, J., Shellnutt, J.G., 2016. Origin of peralkaline granites of the Jurassic Bokan Mountain complex (southeastern Alaska) hosting rare metal mineralization. Int. Geol. Rev. 58, 1–13.
Duncan, R.K., Willett, G.C., 1990. Mount Weld carbonatite. In: Hughes, F.E. (Ed.), Geology of Mineral Deposits of Australia and Papua New Guinea. Australasian Institute of Mining and Metallurgy, 14. Monograph, Melbourne, pp. 591–597.
Eriksson, S.E., 1984. Age of carbonatite and phoscorite magmatism of the Phalaborwa Complex (South Africa). Chem. Geol. 46, 291–299.
Frost, B.R., Barnes, C.G., Collins, W.J., Arculus, R.J., Ellis, D.J., Frost, C.D., 2001. A geochemical classification for granitic rocks. J. Petrol. 42, 2033–2048.
Frost, B.R., Frost, C.D., 2008. A geochemical classification for feldspathic rocks. J. Petrol. 49, 1955–1969.
Frost, C.D., Frost, B.R., 2011. On ferroan (A-type) granites: their compositional variability and modes of origin. J. Petrol. 52, 39–53.
Gladkochub, D.P., Donskaya, T.V., Reddy, S.M., Poller, U., Bayanova, T.B., Mazukabzov, A.M., Dril, S., Todt, W., Pisarevsky, S.A., 2009. Palaeoproterozoic to Eoarchaean Crustal Growth in Southern Siberia: A Nd-isotope Synthesis. 323 Geological Society, London, Special Publications pp. 127–143.
Gladkochub, D.P., Pisarevsky, S.A., Donskaya, T.V., Ernst, R.E., Wingate, M.T.D., Söderlund, U., Mazukabzov, A.M., Sklyarov, E.V., Hamilton, M.A., Hanes, J.A., 2010. Proterozoic mafic magmatism in Siberian craton: An overview and implications for paleocontinental reconstruction. Precambr. Res. 183, 660–668.
Gladkochub, D.P., Pisarevsky, S.A., Donskaya, T.V., Natapov, L.M., Mazukabzov, A.M., Stanevich, A.M., Sklyarov, E.V., 2006. The Siberian Craton and its evolution in terms of the Rodinia hypothesis. Episodes 29, 169–174.
Goldstein, S.J., Jacobsen, S.B., 1988. Nd and Sr isotopic systematics of rivers water suspended material: implications for crustal evolution. Earth Planet. Sci. Lett. 87, 249–265.
Graham, S., Lambert, D., Shee, S., 2004. The petrogenesis of carbonatite, melonite and kimberlite from the Eastern Goldfield Province, Yilgarn Craton. Lithos 76, 519–533.
Gramenitskiy, E.N., Shchekina, T.I., Devyatova, V.N., 2005. Phase Relations in Fluorine-Containing Granite and Nepheline Syenite Systems and the Element Distribution Between Phases (Experimental Research). GEOS, Moscow (in Russian).
Harmer, R.E., 2000. Mineralisation of the Phalaborwa Complex and the carbonatite connection in iron oxide-Cu-Au-U-REE deposits. In: Porter, T.M. (Ed.), Hydrothermal Iron Oxide Copper-Gold and Related Deposits: A Global Perspective. Australian Mineral Foundation, Adelaide, pp. 331–340.
Huang, H., Zhang, Z., Santosh, M., Zhang, D., 2014. Geochronology, geochemistry and metallogenic implications of the Boziguo'er rare metal-bearing peralkaline granitic intrusion in South Tianshan, NWChina. Ore Geol. Rev. 61, 157–174.
Jacobsen, S.B., Wasserburg, G.J., 1984. Sm-Nd isotopic evolution of chondrites and achondrites, II. Earth Planet. Sci. Lett. 67, 137–150.
Jochum, K.P., Dingwell, D.B., Stoll, B., Hofmann, A.W., 2000. The preparation and preliminary characterization of eight geological MPI-DING reference glasses for in situ microanalysis. Geostandarts Newslett. 24, 87–133.
Kotov, A.B., 2003. The boundary conditions of geodynamic models for the formation of the continental crust of the Aldan Shield. ScD thesis. Izd. SPbGU, St. Petersburg (in Russian).
Kotov, A.B., Kovach, V.P., Salnikova, E.B., Glebovitskii, V.A., Yakovleva, S.Z., Berezhnaya, N.G., Myskova, T.A., 1995. Continental crust age and formation stages in the Central Aldan Granulite-Gneiss terrain: U-Pb and Sm-Nd isotopic data for granitoids. Petrology 3, 87–97.
Kotov, A.B., Tolmacheva, E.V., Salnikova, E.B., Velikoslavinsky, S.D., Gladkochub, D.P., Sklyarov, E.V., Donskaya, T.V., Prokopov, N.S., 2015a. New data on the conditions of formation and transformation of the rare metal alkaline granites of the Katugin masif. In: Sklyarov, E.V. (Ed.), Geodynamic Evolution of Lithosphere in the Central Asian Mobile Belt (From Ocean to Continent). ISK SO RAN, Irkutsk, pp. 125–126 (in Russian).
Kotov, A.B., Vladykin, N.V., Larin, A.M., Gladkochub, D.P., Salnikova, E.B., Sklyarov, E.V., Tolmacheva, E.V., Donskaya, T.V., Velikoslavinsky, S.D., Yakovleva, S.Z., 2015b. New data on the age of ore formation in the unique Katugin rare metal deposit (Aldan Shield). Dokl. Earth Sci. 463, 663–667.
Krogh, T.E., 1973. A low-contamination method for hydrothermal decomposition of zircon and extraction of U and Pb for isotopic age determination. Geochim. Cosmochim. Acta 37, 485–494.
Krogh, T.E., 1982. Improved accuracy of U-Pb zircon ages by the creation of more concordant systems using an air abrasion technique. Geochim. Cosmochim. Acta 46, 637–649.
Larin, A.M., Kotov, A.B., Sal'nikova, E.B., Kovalenko, V.I., Kovach, V.P., Yakovleva, S.Z., Berezhnaya, N.G., Ivanov, V.E., 2002. Age of the Katugin Ta–Nb deposit, Aldan-Stanovoi Shield: evidence for the identification of the global rare metal metallogenic epoch. Dokl. Earth Sci. 383, 336–339.
Larin, A.M., Kotov, A.B., Velikoslavinskii, S.D., Sal'nikova, E.B., Kovach, V.P., 2012. Early Precambrian A-granitoids in the Aldan Shield and adjacent mobile belts: Sources and geodynamic environments. Petrology 20, 218–239.
Larin, A.M., Kotov, A.B., Vladykin, N.V., Gladkochub, D.P., Kovach, V.P., Sklyarov, E.V., Donskaya, T.V., Veklikoslavinskii, S.D., Zagornaya, N.Yu., Sotnikova, I.A., 2015. Rare metal granites of the Katugin complex (Aldan Shield): sources and geodynamic formation settings. Dokl. Earth Sci. 464, 889–893.
Levashova, E.V., Skublov, S.G., Marin, Yu.B., Lupashko, T.N., Ilchenko, E.A., 2014. Trace elements in zircon from the rocks of the Katugin rare metal deposit. Zapiski RMO (Proceedings of the Russian Mineralogical Society) 143 (5), 17–31 (in Russian with English abstract).
Ludwig, K.R., 1991. PbDat for MS-DOS, version 1.21. U.S. Geological Survey Open-File Report 88–542.
Ludwig, K.R., 1999. ISOPLOT/Ex.Version 2.06, A Geochronological Toolkit for Microsoft Excel. Berkley Geochronology Center, Berkeley, Special Publication 1a.
Lukkari, S., Holtz, F., 2007. Phase relations of a F-enriched peraluminous granite: An

experimental study of the Kymi topaz granite stock, southern Finland. Contrib. Miner. Petrol. 153, 273–288.
Manning, D.A.C., 1981. The effect of fluorine on liquidus phase relationships in the system Qz–Ab–Or with excess water at 1 kb. Contrib. Miner. Petrol. 76, 206–215.
Markl, G., Marks, M., Schwinn, G., Sommer, H., 2001. Phase equilibrium constraints on intensive crystallization parameters of the Ilímaussaq Complex, South Greenland. J. Petrol. 42, 2231–2258.
Moghazi, A.M., Harbi, H.M., Ali, K.A., 2011. Geochemistry of the Late Neoproterozoic Hadb adh Dayheen ring complex, Central Arabian Shield: Implications for the origin of rare-metal-bearing post-orogenic A-type granites. J. Asian Earth Sci. 42, 1324–1340.
Osokin, E.D., Altukhov, E.N., Kravchenko, S.M., 2000. Criteria and formation and localization conditions of giant rare element deposits. Geol. Ore Deposits 42, 351–357.
Panteeva, S.V., Gladkochoub, D.P., Donskaya, T.V., Markova, V.V., Sandimirova, G.P., 2003. Determination of 24 trace elements in felsic rocks by inductively coupled plasma mass spectrometry after lithium metaborate fusion. Spectrochim. Acta, Part B 58, 341–350.
Pirajno, F., 2009. Hydrothermal Processes and Mineral Systems. Springer, Berlin.
Pirajno, F., 2015. Intracontinental anorogenic alkaline magmatism and carbonatites, associated mineral systems and the mantle plume connection. Gondwana Res. 27, 1181–1216.
Pirajno, F., Santosh, M., 2014. Rifting, intraplate magmatism, mineral systems and mantle dynamics in central-east Eurasia: An overview. Ore Geol. Rev. 63, 265–295.
Podkovyrov, V.N., Kotov, A.B., Larin, A.M., Kotova, L.N., Kovach, V.P., Zagornaya, N.Yu., 2006. Sources and provenances of Lower Proterozoic terrigenous rocks of the Udokan Group, southern Kodar-Udokan depression: results of Sm–Nd isotopic investigations. Dokl. Earth Sci. 408, 223–227.
Pouchou, J.-L., Pichoir, F., 1985. "PAP" (ϕ–ρ–Z) procedure for improved quantitative microanalysis. In: Armstrong, T. (Ed.), Microbeam Analysis. San Francisco Press, San Francisco, pp. 104–106.
Prokhorov, K.V., Sobachenko, V.N., 1985. Structural–petrological and geochemical conditions of the formation of ore-bearing high-temperature sodic metasomatites. In: Tomson, I.N. (Ed.), Inner Structure of Ore-Bearing Precambrian Faults. Nauka, Moscow, pp. 94–121 (in Russian).
Puchtel, I.S., Zhuravlev, D.Z., 1992. Early Proterozoic picrites from Olekma granite-greenstone area - Nd isotope systematics and petrogenesis. Geokhimiya, No 8, 1111–1123.
Rosen, O.M., 2003. Siberian craton: tectonic regionalization and evolution stages. Geotektonika, No 3, 3–21.
Ryabtsev, V.V., Chistov, L.B., Shuriga, T.N., 2006. Tantalum Ores of Russia: State and Prospects of the Development of the Raw Mineral Base. VIMS, Moscow (in Russian).
Scaillet, B., Macdonald, R., 2003. Experimental constraints on the relationships between peralkaline rhyolites of the Kenya rift valley. J. Petrol. 44, 1867–1894.
Scaillet, B., Macdonald, R., 2001. Phase relations of peralkaline silicic magmas and petrogenetic implications. J. Petrol. 42, 825–845.
Schönenberger, J., Köhler, J., Markl, G., 2008. REE systematics of fluorides, calcite and siderite in peralkaline plutonic rocks from the Gardar Province, South Greenland. Chem. Geol. 247, 16–35.
Seltmann, R., Soloviev, S., Shatov, V., Pirajno, F., Naumov, E., Cherkasov, S., 2010. Metallogeny of Siberia: tectonic, geologic and metallogenic settings of selected significant deposits. Aust. J. Earth Sci. 57, 655–706.
Sharpenok, L.N., Kostin, A.E., Kukharenko, E.A., 2013. TAS-diagram alkali sum – silica for chemical classification and diagnostics of plutonic rocks. Regional Geol. Metallogeny 56, 40–50 (in Russian with English abstract).
Sharygin, V.V., Vladykin, N.V., 2014. Mineralogy of cryolite rocks from the Katugin massif, Transbaikalia, Russia. In: Ilbeyli, N., Yalcin, M.G. (Eds.), Abstract Book of 30th International Conference on "Ore Potential of Alkaline, Kimberlite and Carbonatite Magmatism". Akdeniz University, Antalya, pp. 166–168.
Shchekina, T.I., Gramenitskiy, E.N., Alferyeva, Ya.O., 2013. Leucocratic magmatic melts with the maximum fluorine concentrations: experiment and relations in nature. Petrology 21, 454–470.
Sheard, E.R., Williams-Jones, A.E., Heiligman, M., Pederson, C., Trueman, D.L., 2012. Controls on the concentration of zirconium, niobium and the rare earth elements in the Thor Lake rare metal deposit, Northwest Territories, Canada. Econ. Geol. 107, 81–104.
Simonetti, A., Goldstein, S.L., Schmidberger, S.S., Viladkar, S.G., 1998. Geochemical and Nd, Pb and Sr isotope data from Deccan alkaline complexes: inferences for mantle sources and plume-lithosphere interaction. J. Petrol. 39, 1847–1864.
Sklyarov, E.V., Gladkochub, D.P., Kotov, A.B., Starikova, A.E., Sharygin, V.V., Velikoslavinsky, S.D., Larin, A.M., Mazukabzov, A.M., Tolmacheva, E.V., Khromova, E.A., 2016. Genesis of the Katugin rare-metal ore deposit: magmatism versus metasomatism. Russian J. Pacific Geol. 10, 155–167.
Smith, M.P., Moore, K., Kavecsanszki, D., Finch, A.A., Kynicky, J., Wall, F., 2016. From mantle to critical zone: A review of large and giant sized deposits of the rare earth elements. Geosci. Front. 7, 315–334.
Stacey, J.S., Kramers, I.D., 1975. Approximation of terrestrial lead isotope evolution by a two-stage model. Earth Planet. Sci. Lett. 26, 207–221.
Steiger, R.H., Jager, E., 1976. Subcomission of Geochronology: convension of the use of decay constants in geo- and cosmochronology. Earth Planet. Sci. Lett. 36, 359–362.
Sun, S., McDonough, W.F., 1989. Chemical and isotopic systematics of oceanic basalts: implications for mantle composition and processes. In: In: Saunders, A.D., Norry, M.J. (Eds.), Magmatism in the Oceanic Basins Geol. Soc. London. Spec. Publ. 42, pp. 313–345.
Trueman, D.L., Pedersen, J.C., de St. Jorre, L., Smith, D.G.W., 1988. The Thor Lake rare-metal deposits, Northwest Territories. In: In: Teilor, R.P., Strong, D.F. (Eds.), Recent Advances in the Geology of Granite-related Mineral Deposits Vol. 38. The Canadian Institute of Mining and Metallurgy, Sp., pp. 280–290.
Wakita, H., Schmitt, R.A., Rey, P., 1970. Elemental abundances of major, minor, and trace elements in Apollo 11 lunar rocks, soil and core samples. Proceedings of the Apollo 11 Lunar Science Conference, pp. 1685–1717.
Webster, J., Thomas, R., Förster, H.J., Seltmann, R., Tappen, C., 2004. Geochemical evolution of halogen-enriched granite magmas and mineralizing fluids of the Zinnwald tin– tungsten mining district, Erzgebirge, Germany. Miner. Deposita 39, 452–472.
Webster, J.D., 1990. Partitioning of F between H_2O and CO, fluids and topaz rhyolite melt. Contrib. Miner. Petrol. 104, 424–438.
Webster, J.D., Holloway, J.R., Hervig, R.L., 1989. Partitioning of lithophile trace elements between H_2O and $H_2O + CO_2$ fluids and topaz rhyolite melt. Econ. Geol. 84, 116–134.
Whitmeyer, S.J., Karlstrom, K.E., 2007. Tectonic model for the Proterozoic growth of North America. GSA Bull. 3, 220–259.
Xiong, X.-L., Zhao, Z.-H., Zhu, J.-C., Rao, B., 1999. Phase relations in albite granite-H_2O-HF system and their petrogenetic applications. Geochem. J. 33, 199–214.
Yin, J.W., Shao, X.K., Yang, H.T., Piao, T.X., Xu, H.M., Wang, J., 2013. Radioactive mineral characteristics of Boziguoer alkaline rocks in Baicheng, Xinjia. Mineral Deposits 32, 337–352.